DESIGN OPTIMIZATION OF WHEEL-AND-LEG TRANSFORMABLE ROBOT WITH PASSIVE ACTUATION

A Thesis

by

SIDDHARTH NITIN SANE

Submitted to the Office of Graduate and Professional Studies of
Texas A&M University
in partial fulfillment of the requirements for the degree of

MASTER OF SCIENCE

Chair of Committee,	Kiju Lee
Committee Members,	Srikanth Saripalli
	Xingyong Song
Head of Department,	Andreas A. Polycarpou

May 2021

Major Subject: Mechanical Engineering

ABSTRACT

This thesis presents design optimization and hardware development of a new small-size Unmanned Ground Vehicle (UGV) equipped with novel wheel-leg transformable mechanisms for enhanced, adaptive ground locomotion. The design of the transformable wheels is based on a previously developed Wheel-and-Leg Reconfigurable (WheeLeR) mechanism proposed for microrobots. Engineering challenges involved with physical scaling-up of this passive mechanism into a fully functional UGV is addressed by Multidisciplinary Design Optimization, design of a suspension system, and hardware development. Passively transformable wheels of this mobile robotic platform can be customizable to suit different types of terrains and have a capability to climb intermediate and continuous obstacles, such as staircases. The factors affecting the transition between wheel-and-legs are identified and optimized by design space exploration and gradient descent algorithm. The dimensions of the robotic platform are optimized by multi-objective optimization to achieve the objectives of minimizing the torque required for the robot to climb a staircase and maximizing the gradient of the ascent of the robot while climbing up or down an obstacle without turning over. Post optimality analysis provides insights into the effects of variables and parameters on these objectives. Design, manufacture, and assembly of the chassis and the wheels with proper sensor configuration and electronic layout completes the process of scaling-up to develop a fully functioning robotic platform with optimal and reliable performance.

DEDICATION

To my parents

ACKNOWLEDGEMENTS

First, I would like to thank my committee chair, Dr. Lee, for her diligent support and guidance throughout the course of this research. I would like to express my sincere gratitude towards her for giving me this opportunity and for believing in me. Her optimism, perfectionism and expansive knowledge have deeply inspired me. I have always considered myself lucky to be able to work with her for the past two years. I would like to thank my committee members, Dr. Saripalli and Dr. Song for their timely help and feedback.

I also thank my colleagues from Adaptive Robotics and Technology (ART) Lab for enhancing my knowledge and skills vastly, developing team spirit and making the experience at Texas A&M University enlightening and enjoyable. A special thanks go to my friends who have made this journey worthwhile.

I extend my gratitude towards my relatives, near and far, who have always wished the best for me.

Finally, I am immensely grateful towards my parents and my sister for their unwavering support, motivation, and love throughout my graduate education.

I feel humbled to have all these people in my life who have made it fulfilling and enriching.

CONTRIBUTORS AND FUNDING SOURCES

Contributors

The spring-suspension system for the transformable wheel mechanism presented in Chapter VII was developed in collaboration with Chuanqi Zheng.

The final prototype of the project presented in Chapter VIII is a collaborative effort by Chuanqi Zheng, Kangneong Lee, Vishnu Kalyanram, and Jenna Horn of Department of Mechanical Engineering.

All other work conducted for the thesis is completed by the student independently.

Funding Sources

This work is made possible by Defense Advanced Research Projects Agency (DARPA), under Grant Number HR00112020037, in OFFSET Sprint-5 program. Its contents are solely the responsibility of the author and do not necessarily represent the official views of DARPA.

NOMENCLATURE

UGV	Unmanned ground vehicle
MDO	Multidisciplinary design optimization
MSADO	Multidisciplinary system analysis and design optimization
r_1	Radius of central gear
r_2	Radius partial gear
r_{sum}	Sum of radii of central and partial gears
k	Coefficient of rolling friction
p	Gear ratio between partial gear and central gear
θ	Angle with which leg hits ground
n	Number of factors in full factorial design
l	Number of levels in full factorial design
e	Number of experiments in full factorial design
x_{opt}	Optimal output vector
J_{opt}	Optimal objective function
S_N	Normalized sensitivity vector
L	Length of chassis
W	Width of chassis
H	Height of chassis
t	Thickness of chassis wall
w	Wheel width

ρ	Density of chassis material
P	Payload
SSF	Static stability factor
δ	Deflection of chassis
E	Modulus of elasticity
I	Moment of inertia
g	Gravitational acceleration
CG	Center of gravity
COM	Center of mass
h	Height of CG from ground
m	Mass of vehicle
β	Angle of slope
F	Frictional force
μ	Coefficient of kinetic friction
L_{CG}	Longitudinal position of CG
V_{CG}	Vertical position of CG
x	Fraction of length of chassis
S_{yt}	Yield strength
S_{ut}	Ultimate tensile strength
fs	Factor of safety
σ_t	Permissible stress
σ_b	Bending stress

M_b	Bending moment
K_i	Wahl factor
C	Spring index
d	Wire diameter
D	Outer diameter
CAD	Computer aided design
IMU	Inertial measurement unit
USB	Universal serial bus
CAN	Controller area network
GPIO	General purpose input/ output
UART	Universal asynchronous receiver-transmitter
I2C	Inter-integrated circuit
GPS	Global positioning system
GNSS	Global navigation satellite system
LiDAR	Light detection and ranging
PLA	Polylactic acid (3D printing filament material)
SMA	Sub-miniature version A (cable)
GPU	Graphics processing unit
ROS	Robot operating system

TABLE OF CONTENTS

Page

LIST OF FIGURES

Page

LIST OF TABLES

Page

CHAPTER I

INTRODUCTION

The chapter 1) presents an overview of existing work in the area of wheel-leg transformable robots and recent trends in the mobile robots with enhanced locomotion capabilities; 2) introduces the "WheeLeR" mechanism which forms the technical groundwork of this thesis project; and 3) summarizes technical contributions of this thesis, in particular related to physical scaling-up of a proof-of-concept prototype to a fully equipped Unmanned Ground Vehicle (UGV) for real-world applications.

1.1 Background

Mobile robots are intelligent machines controlled by software to navigate through the environment. They have the capability of locomotion as against most of the industrial robots with a robotic arm or a gripper with a fixed base. A UGV is a subset of mobile robots, operating autonomously, while in contact with the ground. The most common modes of locomotion are wheels [1] [2], legs [3] [4], and tracks [5] [6]. Wheels are considered the most efficient and the simplest method of locomotion for the robots traversing on relatively smooth and solid surface. However, they may show difficulties on rough, rugged, or soft terrains. The legged locomotion found in most of the biological systems, allows a robot to traverse not only on these challenging surfaces but also on

intermediate obstacles and continuous obstacles (e.g., stairs). However, legged robots have complex mechanical design, typically require advanced control algorithms, and demand generation of appropriate gait for locomotion. They also tend to have lower speeds and higher cost of manufacturing as compared to their wheeled counterparts. Robots with tracks can overcome obstacles and soft terrains better than the wheeled robots but suffer from low speeds and low maneuverability due to their complex mechanical design. The tracked robots also have higher failure rates which demands for higher maintenance. A robot having a capability to transition between the two or more modes can potentially offer an effective solution for applications that involves different types of terrains and obstacles. Existing robots with such transformation capabilities mostly focus on wheel-leg transformation that can be divided into those with an active transformation system and the others which rely on passive transformation.

Robots with an active transformation mechanism involve an additional actuator(s) for triggering the transition between the two locomotion modes. A circular pattern of leg segments around a disk that open or close when the disc exerts a pull, or a push and related designs are presented in [7] [8] [9] [10] [11] [12]. Another design involves having two semicircular wheels forming a single semicircular leg [13] [14] or it can also have two semicircular segments opening to form two legs [15]. Transleg is another model which uses a wire-spring couple to switch between wheel-and-leg mode [16]. A wheel-track-leg based system operating with foldable rims is also presented in [17]. Another design uses pneumatic actuators to change the diameter of the wheel [18]. Some other active actuator solutions based on biomimetics like an Armadillo [19] or a non-transformable rough

terrain traversing snake robot is given in [20]. A complex wheel-leg transformation mechanism is shown in AZIMUT [21], PAW [22], FUHAR [23], Claw-Wheel robot [24], and STEP [25]. All these robots have one or more actuators triggering the mode switch. This results in higher consumption of energy and complicated mechanical assembly and control.

Passive transition relies on external and/or internal factors without active control. This has been a relatively unobserved area of research. There are only a few robots developed with this type of actuation. Passive mechanisms take advantage of different terrain conditions or of unique mechanical designs involved to trigger the change from wheel to leg and vice versa, e.g., Wheel Transformer [26]. Another form of passive actuation is to have a spoke frame with wheels on its end and the whole spoke frame rotates to have legged locomotion, called Tri-wheel [27]. One of the designs uses coupling of centrifugal force with magnet while the springs trigger flipping between wheels and legs, but it requires a run-up to initiate switching [28]. An optional active/ passive mechanism with four bar linkage is represented in [29]. A curved spoke frame used to climb staircases presented in [30] does not have the ability to switch to another mode on flat surfaces. The simulations of the four-link mechanism [31] and a trajectory planning based concept of an adaptable wheel [32] are also previously studied. A robot dog Karaw which opens its thighs and shanks to switch to wheeled mode is proposed in [33]. All of these have a relatively complex switching mechanism.

1.2 Concept of Wheel-Leg Transition

The primary objective of this thesis is to successfully engineer the previously developed proof-of-concept prototype WheeLeR [34] into a mobile robotic platform with embedded autonomous navigation system that can be used for practical applications. Therefore, it is important to review the original design of WheeLeR – a unique wheel-leg transition mechanism that is triggered passively [34]. The WheeLeR mechanism consists of a central gear which is the driving gear and different number of partial gears which are the driven gears (**Figure 2 (a)** and **(b)**). The entire structure is then held by two spoke frames which are bolted together. A hub connects the central gear to the motor shaft securely. When the motor shaft is moving in counterclockwise direction, the partial gears remain closed as the clockwise torque on every partial gear is cancelled out by the reactive torque produced by the adjacent partial gear. However, when the motor shaft rotates in clockwise direction, the partial gears rotate in counterclockwise direction which opens the legs as the net torque on the partial gears is now in the opposite direction. This transition is affected by the following factors:

1) Sense of rotation of the motor shaft
2) Terrain conditions and rolling friction
3) Gear ratio
4) Dimensions of the gears

The number of partial gears is customizable and affect the gear ratio and the dimensions of the gears which in turn affects the transition mechanism as well. **Figure 1** shows the

fully assembled prototype with two wheels and a balancing tail. This small-sized prototype is $115 \times 47 \times 31\ mm^3$ (without tail). The robot weighs 400 g.

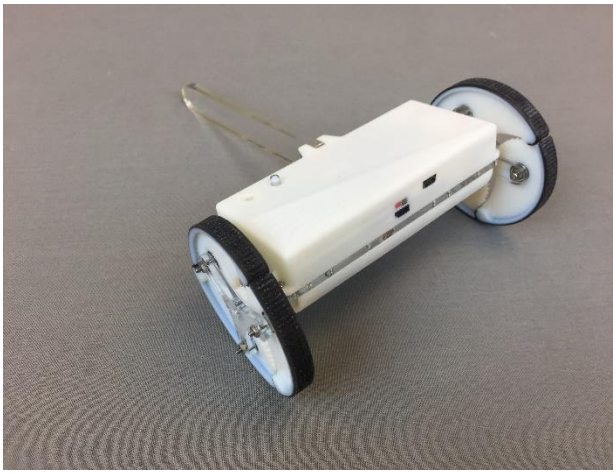

Figure 1. *Prototype of WheeLeR used for a small mobile robot (Image courtesy: [34])*

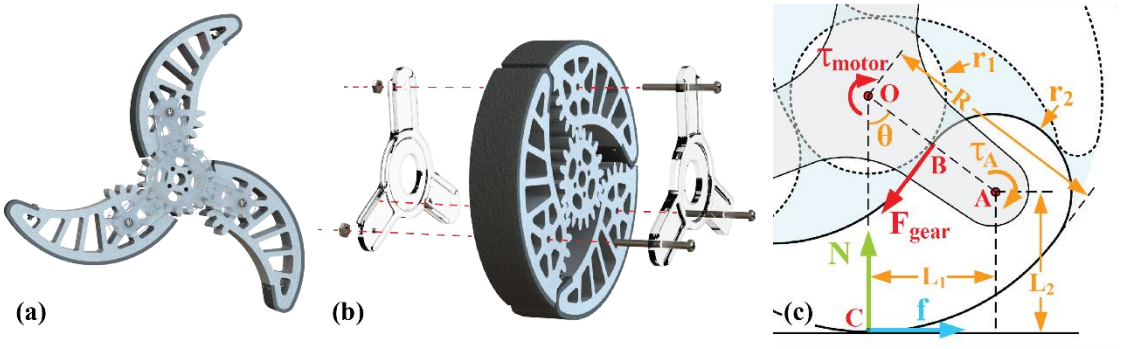

Figure 2. *Fully assembled wheel (a), exploded view of components (b), free body diagram of partial gear (Image courtesy: [34])*

1.3 Scaling-up the Robotic Platform

The new UGV presented in this thesis is an adaptive wheel-leg transformable robot, called *α-WaLTR*, with the same passive transformation capability as WheeLeR. Physical scale-up involves many engineering processes: 1) modifying the current design to be equipped with four wheels (instead of two wheels with a balancing tail) for stability; 2) optimizing the dimensions of the platform to provide the best performance; 3) redesigning the central gear, legs, spoke frames, and chassis with new dimensions; 4) calculating torque and current requirements; 5) analyzing the position of center of gravity and its effects; 6) providing suspension system to absorb the impacts; 7) adding and configuring sensors to automate the robot; 8) developing advanced control algorithms to make it fully autonomous; and finally 9) testing and evaluating its functions.

Multidisciplinary design optimization (MDO) considers all the areas involved in the system simultaneously to determine a global optimum which supersedes all the local optima found through individual disciplines [35]. The scaling process will alter some of the governing equations of motion while keeping the transitioning equations from wheeled to legged mode the same. To determine the optimum parameters of the platform under the constraints of dimensions and terrains, MDO is used. The importance of MDO to implement on complex system is discussed in [36] while its benefits in practical applications are summarized in [37]. The single objective optimization is performed by the reduced gradient method while Pareto front is suited for multi-objective optimization [38].

The process of physical scale-up of WheeLeR is not only necessary for improving overall performance to climb higher obstacles but also makes it more viable for various mobile robot applications, such as search and rescue, navigation, and emergency services, with embedded sensing and processing capabilities. The primary objective of this scale-up is to achieve versatile locomotion capabilities in urban environments. A staircase is a common type of terrain found in urban environments. Each multi-story building is equipped with both indoor and outdoor staircases. A surveillance robot must be able to traverse upper floors for monitoring and inspection. Additionally, scoping indoor environment with drones may be complicated. A ground rover with necessary payload capable of climbing staircases can be more useful and practical in these cases. To enable the robot to traverse up/down staircases as well as other types of common terrains (e.g., slopes, grass, flat, and gaps), this thesis focuses on the following engineering challenges involved with physical scale-up:

1) Requirement for higher frictional grip between wheels and the ground and its effect on the transition mechanism.
2) Increase in the weight of the robot.
3) Balancing to avoid toppling while climbing obstacles.
4) Increase in the inertia forces and vibrations due to the weight and additional payload affecting structural durability and sensing performance.
5) Configuring sensing elements and microcontroller as the bigger platform demands more complex control algorithms.

These challenges can be addressed by methods of design optimization or by developing a system specifically addressing a particular problem only. This thesis presents a comprehensive approach based on multidisciplinary system analysis adopted for design optimization. This optimization aims to achieve desired locomotion capabilities while minimizing the overall size and weight to make the performance of the robotic platform optimal.

1.4 Specific Aims

This thesis presents a methodology to effectively solve each complication involved with scaling up of the robotic platform. Five specific aims of this thesis are listed below. Detailed technical descriptions for individual objectives are provided in subsequent chapters with the conclusions summarized at the end of each chapter.

Aim 1. *Investigate relationship between the WheeLeR design and wheel-leg transformation behavior.*

The first objective of the thesis is to investigate the transition mechanism between wheel and legs. It is important to understand the factors affecting this transition and thus to select a set of parameters that can effectively achieve the desired transformation tendency. This can be determined by optimization techniques introduced in Chapter II.

Aim 2. *Optimize the chassis dimensions.*

The size of the chassis affects the overall size of traversable obstacles as well as the weight of the robot. Therefore, it is necessary to select optimal dimensions of the chassis. Minimizing the torque required to climb the stairs not only reduces the power consumption but also increases the speed of the robot, and thus it can lead to reduction in its weight. Chapter III describes how to calculate the most effective set of dimensions of the robot chassis that achieve this objective.

Aim 3. *Optimally determine the center of gravity location.*

Furthermore, the increment in weight also affects the stability of the robot as it climbs stairs or obstacles without flipping over. Chapter IV presents the method for locating the optimal position of the center of gravity of the robot to maximize its ability to ascend relatively higher slopes without toppling with dynamic analysis and optimization techniques.

Aim 4. *Develop embedded spring suspension system for transformable wheels.*

Another objective is to design a mechanical suspension system to absorb vibrations. As the weight of the robot increases so do the impact forces. Moreover, bigger legs also contribute to a higher position of center of gravity resulting in higher vibrations in the robot as the legs hit the ground. Chapter V devices a suspension system to absorb the vibrations and provide smoother performance.

Aim 5. *Construct a fully assembled and equipped UGV based on optimization.*

Lastly, as the robotic platform gets mechanically complicated, it demands for complex control. Thus, the robot needs to be equipped with sensors which will enable it to maneuver autonomously. The sensors need to be configured to work with the processing unit and the connections must be up to their specifications. Moreover, an elegant yet robust chassis needs to be designed to contain the electronics, power system, drive system and the processing unit. It is also essential to create sensor mounts at appropriate locations to secure the sensing elements and allow a smoother operation. This is described in Chapter VI.

CHAPTER II

DESIGN OPTIMIZATION OF TRANSITION MECHANISM

The primary objective of the design space exploration in this chapter is to reduce the torque required for wheel-to-leg transition. Wheel-to-leg transition must occur passively while the robot attempts to traverse on non-uniform terrains or obstacles. Since there are multiple variables involved in the analysis of the transition mechanism, the design space is vast. Optimization can point the designer into a direction leading towards the optimal performance of the robot. It can also show the relationship of variables with each other and how changing one affects the other or the objective of the optimization. The post optimality analysis provides the designer an idea of flexibility of each variable in the design space. A flexible variable can have different values and not impact the objective function. However, a variable with dominant impact must not be altered significantly as it can result in drastic changes to the objective function.

2.1 Objective

This optimization aims to minimize the torque required to switch between two modes. The torque between the wheel and legged mode is a function between the dimensions of the wheel, the coefficient of rolling friction, and the gear ratio between the central and partial gears. The derivation of the function depends on the dynamic analysis

of WheeLeR [34]. The function $\varphi(k, p, r_{sum}, \theta)$ below must be as small as possible to minimize the torque requirement:

$$\varphi(k, p, r_{sum}, \theta) = r_{sum}.\, sin\,\theta - k\left(1 + p - \frac{(p+1).\, cos\theta}{(2p+1)}\right) \qquad (0\text{-}1)$$

where r_{sum} is the sum of the radius of central gear (r_1) and the radius of the partial gear (r_2), p ($= r_2/r_1$) is the gear ratio between r_1 and r_2, θ is the angle between the center of the partial gear with the vertical from ground, and k the coefficient of friction between the partial leg and the ground. **Figure 2(c)** shows the radii of the central and partial gear with the frictional force acting between the leg and the ground.

2.2 Assumptions

The angle with which the leg hits the ground (θ) cannot be controlled and hence is considered fixed at 45°. This assumption leads for the objective function in (**0-1**) to have only three variables, i.e., r_{sum}, k and p. Also, the normal force on the leg cannot be calculated and thus excluded from the optimization. The function in (**0-1**) is directly proportional to the torque and thus affects it linearly. In summary, the normal force is given; and the angle between the center of the partial gear and vertical line continuously varies and is not considered in the optimization as it cannot be controlled by the user.

2.3 Constraints

Each optimizable variable is constrained in the design space. These constraints can be of limitations of the user or manufacturer or demanded by the system. One may also

force certain constraints on the variables for desired outcome and performance. One of the most fundamental constraints is the bounds on a variable. For example, r_{sum} in the case of the objective function is bounded by lower and upper allowable values. A wheel cannot be too small nor too large. This constraint is set by the user based on their requirements. Constraints can differ depending on factors such as the application, operation environment, and cost. In this project, the upper and lower bounds were specified as 90mm and 70mm, respectively, such that

$$70\ mm \leq R \leq 90\ mm$$

where $R\ (= r_1 + 2r_2)$ is the total wheel radius.

Given the lower and upper bound of the radius of wheel fixed, the gear ratio p may vary. The gear ratios are chosen from the standard series of 0.5, 1, 1.5, 2, 2.5, 3, 4, 5 and so on [39]. For a gear ratio of less than one, the input torque is not amplified as the number of teeth on the output gear are less than the input gear. For the mechanical advantage and the geometric design constraints of WheeLeR, the following three cases of the p values were considered:

- $\underline{p = 1}$: $23 \leq r_1 \leq 30;\ 23 \leq r_2 \leq 30;\ 46 \leq r_{sum} \leq 60$
- $\underline{p = 1.5}$: $17.5 \leq r_1 \leq 22.5;\ 26.25 \leq r_2 \leq 33.75;\ 43.75 \leq r_{sum} \leq 56.25$
- $\underline{p = 2:}$ $14 \leq r_1 \leq 18;\ 28 \leq r_2 \leq 36;\ 42 \leq r_{sum} \leq 54$

As observed from the above three cases, selecting the permissible range of r_{sum} satisfying all cases yields to $46 \leq r_{sum} \leq 54$.

The coefficient of rolling friction (k) depends on the material used on the wheels which comes in contact with the ground and the ground itself. The values of the common

coefficients are provided in **Table 1.** The coefficient of rolling friction varies between 0.0001m and 0.01m. Therefore, these bounds are considered for k, such that $10^{-4} \leq k \leq 10^{-2}$.

All the variables now have lower and upper bounds and have specific ranges in which they can be varied.

Table 1. *Coefficients of rolling friction for common terrains.*

No	Condition	Terrains	Value in meters
1	Wheels without any friction material added	Hard floor; Concrete; New asphalt	3×10^{-4}
2	Wheels with friction material on surfaces with minor irregularities	Hard floor; Concrete; New asphalt	1.5×10^{-3}
3	Wheels with friction material on surfaces with moderate irregularities	Old asphalt; Wet sand/ground	2.5×10^{-3}
4	Wheels with friction material on surfaces with major irregularities	Rugged; Loose sand/dirt	0.02

2.4 Design Space Exploration

Once the constraints have been identified, the parameters associated in the design space exploration can be selected [38]. Any method based on the exploration consists of two main parameters. The first parameter is the number of variables involved in the design space. In this case, the variables are r_{sum}, p, and k. The second parameter is the number of levels included in the exploration. This essentially discretizes the range of each variable

into certain smaller sections. Since the current problem considers three allowable values of the gear ratio p (=1, 1.5, or 2), the levels associated with this are three. The same number is selected for the other two variables for consistency. This means that r_{rum} is changing from 46mm to 54mm in three stages. The first level can be taken as 46mm, the second level as 50mm and the third level as 54mm. k can also be discretized in three categories of 0.0001, 0.001 and 0.01m. This can be summarized as

- n (Number of the factors) = 3
- l (Number of the levels considered) = 3

Now that the factors and levels are determined, the number of experiments can be calculated by simply taking the number of levels as the index of number of variables:

- e (Number of experiments) = $n^l = 27$

This means that there are 27 possible ways to select the variables leading to 27 values of the objective function. Based on this process, an optimal set of variables that minimizes the objective function can be determined.

Full Factorial Design

This method considers all possible design conditions—which are 27 in this problem—and helps to choose the optimal combination of factors and their respective levels. This method is preferred over Orthogonal Arrays and Parameter studies. The Orthogonal Arrays are used for design spaces with a large number of variables where considering all possible combinations of the variables with the objective function is computationally heavy and time consuming. For example, a design space with 6 factors

and 5 levels yields to a combination set of 7776 levels which is computationally exhaustive. In this case, a set of predefined combination of factors and parameters are selected to represent the entire design space.

If one were to use Orthogonal arrays for the concerned design problem, the 7776 combinations would have been represented by a certain number of combinations (25) based on number of factors and number of levels. These arrays are called as Taguchi Arrays [40]. The method of Orthogonal arrays is less accurate as it does not explore each and every level possible combination in the design space but rather gives an overall idea of the trends between the variables and objective function which in most of the cases is sufficient to converge towards optimal solution. Since there are only 27 experiments in the current design problem, the full factorial arrays are used for better accuracy. **Table 2** shows the array with three levels and three factors expressed in a tabular format.

Table 3 shows the results from the 27 experiments with all combinations considered. The first column is of the number of experiments, the next three are of the factors. The fifth column calculates the objective function and the designer tries to find minimum from all the rows. The last column assigns a normalized score to each row, ranging from zero to unity. This score is calculated by dividing each row in the function column with the maximum value. It shows that having the highest value of k along with highest p, but the lowest r_{sum} gives the best outcome, i.e. the minimum required torque. It is also worth noting that the variables seem to converge to their upper bounds in case of p and k and, to the lower bound in case of r_{sum}. Therefore, if the ranges of these variables are changed, they will converge to those particular values.

Table 2. *Full factorial array*

Factor	**Level 1**	**Level 2**	**Level 3**
k	0.0001	0.001	0.01
p	1	1.5	2
r_{sum}	0.046	0.05	0.054

Table 3. *Calculations of experiments in objective space*

Experiment	$\boldsymbol{k}$	$\boldsymbol{p}$	$\boldsymbol{r_{sum}}$	**φ**	**N**
1	0.0001	1	0.046	0.032	0.85
2	0.0001	1	0.05	0.035	0.92
3	0.0001	1	0.054	0.038	1.00
4	0.0001	1.5	0.046	0.032	0.85
5	0.0001	1.5	0.05	0.035	0.92
6	0.0001	1.5	0.054	0.038	0.99
7	0.0001	2	0.046	0.032	0.84
8	0.0001	2	0.05	0.035	0.92
9	0.0001	2	0.054	0.038	0.99
10	0.001	1	0.046	0.031	0.81
11	0.001	1	0.05	0.034	0.89
12	0.001	1	0.054	0.036	0.96
13	0.001	1.5	0.046	0.030	0.80
14	0.001	1.5	0.05	0.033	0.87
15	0.001	1.5	0.054	0.036	0.95
16	0.001	2	0.046	0.030	0.78
17	0.001	2	0.05	0.033	0.86
18	0.001	2	0.054	0.035	0.93
19	0.01	1	0.046	0.017	0.45
20	0.01	1	0.05	0.020	0.52
21	0.01	1	0.054	0.023	0.60
22	0.01	1.5	0.046	0.012	0.31
23	0.01	1.5	0.05	0.015	0.38
24	0.01	1.5	0.054	0.017	0.46
25	**0.01**	**2**	**0.046**	**0.007**	**0.17**
26	0.01	2	0.05	0.009	0.25
27	0.01	2	0.054	0.012	0.32

2.5 Effects

The effects are calculated after the experiments have been performed. The effects help to quantify the transition from one level to another level as well as the transition between factors themselves. This means that if one changes a factor from one level to another, the effect will give a number as to how much that will affect the objective.

Table 4 shows the effects of each factor at each level, associated with the full factorial array. For each factor the average value of the function at that level is calculated. For example, for k at the first level with its value of 0.0001, all the values of the objective function corresponding to this are averaged. This leads to the value of 0.0350. Similarly, rest of the values are calculated. The mean value is the average of the entire column of objective function. A lower value indicates that it is not advisable to change the value of that factor from the existing level.

Next, the mean of the objective functions is subtracted from each cell to find out the effects of levels. This shows the averaged response of a factor when its level is changed. **Table 5** displays how each factor affects the objective function at each level.

Lastly, the main effects given in **Table 6**, denote the quantifiable advantages of switching between two levels and whether the switching is justifiable for the user. For example, if designer changes the value of k from level 1 to level 2 (i.e., from 0.0001 to 0.001), it offers only an advantage of 0.0018; whereas, if designer were to change it from level 1 to level 3 (i.e. from 0.0001 to 0.001), the advantage offered would be 0.0203—almost 10 times higher. Similarly, each factor at each level can be examined.

Table 4. *Mean of levels*

Factor	Level 1	Level 2	Level 3
k	0.0350	0.0331	0.0146
p	0.0295	0.0276	0.0256
r_{sum}	0.0248	0.0276	0.0304
Mean	**0.0276**		

Table 5. *Effects of levels*

Factor	Level 1	Level 2	Level 3
k	0.0074	0.0055	-0.0129
p	0.0019	0.0000	-0.0019
r_{sum}	-0.0028	0.0000	0.0028

Table 6. *Main effects*

Factor	L1 to L2	L1 to L3	L2 to L3	Result
k	0.0018	0.0203	0.0185	L3
p	0.0020	0.0039	0.0019	L3
r_{sum}	-0.0028	-0.0056	-0.0028	L1

Interpretations

The main effects give insights into the correlation between factors and objective function. The main interpretations are listed below:

1) A switch from level 1 to any of the higher level is beneficial. Switching from first level to third level is 10 times advantageous than switching to the second level.
2) A switch from the second level to third level is beneficial though not as promising as from the first level.
3) For frictional coefficient, switching between levels is significant as higher levels offer bigger advantage.
4) For the gear ratio it is desired to transit from lower levels to higher levels but the change is not as high as seen in the levels of frictional coefficient.

5) The sum of radii does not contribute to the output and does so negligibly. It is still better to select lower values, i.e., the first level than the second and third levels.

Ultimately, analysis of effects also suggests having highest coefficient of friction and gear ratio and lowest sum of radii. It also hints that the sum of radii doesn't affect the objective as much as the other two factors.

2.6 Optimization by Steepest Gradient Method

The method of steepest gradient descent is used to converge to the optimal solution. This is achieved by taking a small step in local space in the direction of maximum descension. After repeating this process for several iterations one can reach the local minima. The results displayed in **Figure 3** are achieved from the MATLAB codes. The figure on top shows how the value of the objective function decreases and converges to minima per iteration. The bottom figure shows the three variables at their optimal values.

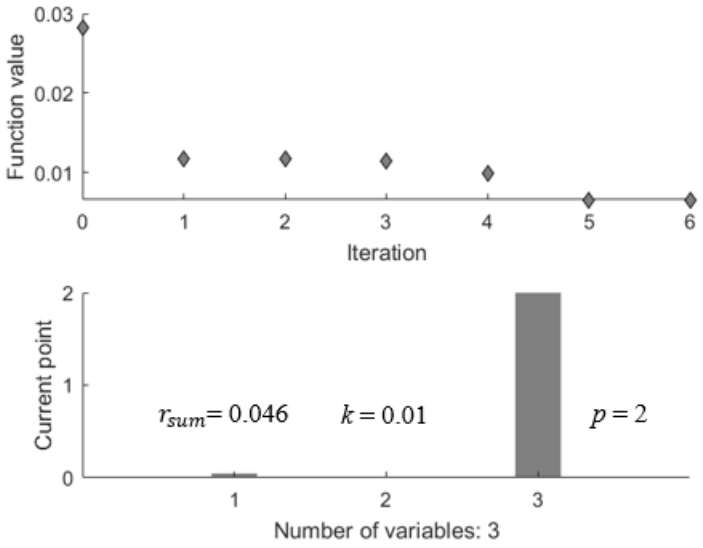

Figure 3. Results of optimization: objective function (top), variables (bottom)

Optimal Output Vector

The optimal output vector can be determined by the steepest gradient method and is expressed as,

$$\boldsymbol{x_{opt}} = \begin{bmatrix} 0.01 \\ 2.0 \\ 0.046 \end{bmatrix} = \begin{bmatrix} k \\ p \\ r_{sum} \end{bmatrix}$$

The highest gear ratio is advisable as it reduces the torque required to transition from wheel to legs. This is reasonable as having a lower gear ratio allows the robot to open legs only when sufficient friction is available, or an obstacle is encountered. In this case, the robot with a higher gear ratio will immediately open the legs when the sense of rotation is changed. Higher rolling friction enables robot to shift from wheel to legs easily.

2.7 Post Processing

Post processing offers a quantitative analysis to determine the effects of variables on the objective space. The detailed process and steps involved in the analysis are described in Chapter VI.

2.7.1 Sensitivity Analysis

The sensitivity analysis quantifies the effect of a variable on the objective function. It helps to focus on certain variables for optimization and to be able to denote lesser important variables. Manually, the sensitivity can be found out by calculating the gradient of the objective function with respect to each variable. This essentially determines the change in the value of the objective function with respect to the change in the variable.

Let ***J*** be the objective function, given by

$$J = r_{sum}.\sin\theta - k\left(1 + p - \frac{(p+1).cos\theta}{(2p+1)}\right)$$

$$J_{opt} = 6.77 \times 10^{-3}$$

$$\frac{\partial J}{\partial k} = -\left(p + 1 - \frac{(p+1).cos\theta}{(2p+1)}\right);\ \frac{\partial J}{\partial p} = -k.\left(1 + \frac{cos\theta}{(2p+1)^2}\right)$$

$$\frac{\partial J}{\partial r_{sum}} = \sin\theta$$

Now at the optimal position $\boldsymbol{x_{opt}}$, we obtain:

$$\boldsymbol{\nabla J} = \begin{bmatrix} -2.576 \\ -0.00964 \\ 0.7071 \end{bmatrix}$$

2.7.2 Normalization

This process converts each coefficient of sensitivity in a range that is comparable with other variables. In this way, comparing the coefficients becomes easier. Each value of the sensitivity gradient is multiplied by its corresponding optimal value and divided by the value of the objective function at the optimal solution.

The normalized sensitivity vector is shown below:

$$\boldsymbol{S_N} = \frac{1}{J_{opt}}\begin{bmatrix} x_{opt_{11}}.\nabla J_{11} \\ x_{opt_{21}}.\nabla J_{21} \\ x_{opt_{31}}.\nabla J_{31} \end{bmatrix} = \begin{bmatrix} -3.8 \\ -2.85 \\ 4.8 \end{bmatrix} \quad (0\text{-}2)$$

The negative sign indicates that increasing that variable will decrease the objective function as observed earlier. Similarly, for r_{sum}, an increment results in an increase of the objective function. k has the highest impact on the objective function while p also affects the objective considerably.

In summary, the optimization of the transition mechanism shows the impact of each variable on the performance of the robot. Having a higher gear ratio allows the wheels to switch to the leg configuration immediately after changing the direction of rotation while a lower gear ratio can allow the switch only when an obstacle is encountered. The torque of transition is minimum when r_{sum} is at its minimum value. Also, the torque is the lowest when the robot moves on a highly rough surface as it aids the switching from wheels to legs.

CHAPTER III

OPTIMIZATION OF CHASSIS DIMENSIONS

The chassis dimensions not only affect the weight of the robot but also its stability. To develop an objective function with necessary constraints, a simple equation of motion, i.e., the torque required to climb an obstacle, is used. For the robot to be able to climb stairs successfully, it is important to have motors which are powerful enough to carry the weight of the robot by creating sufficient torque. However, the higher the torque of the motor, the lower its speed and the higher the weight of the motor itself. Thus, an optimal set of variables can minimize the torque required to climb the stairs and can locate a satisfactory trade-off between torque and speed characteristics of the motor. The motor selection is explained in Chapter VIII.

3.1 Variables and Parameters

The variables and parameters involved in this optimization process are displayed in the **Table 7** and **Table 8**, respectively. The variables and parameters are also visualized in **Figure 4**. The variables are the values that are found through various techniques of optimization while parameters are the values which are predetermined in an optimization process. The categorization of variables and parameters is based on the requirements of the robot and availability of pre-determined data. For example, the values of overall

dimensions of chassis cannot be predetermined but can be constrained to find the optimal values in their respective ranges. Thus, they are considered as variables.

Table 7. *List of variables*

No	Variable	Symbol	Representation
1	Length of the Chassis	*L*	*x(1)*
2	Width of the Chassis	*W*	*x(2)*
3	Height of the Chassis	*H*	*x(3)*
4	Thickness of the Chassis Wall	*t*	*x(4)*
5	Radius of the Central Gear	r_1	*x(5)*
6	Radius of the Partial Gear	r_2	*x(6)*

Table 8. *List of parameters*

No	Parameter	Symbol
1	Wheel Width	*w*
2	Density of the Chassis Material	*ρ*
3	Payload	*P*

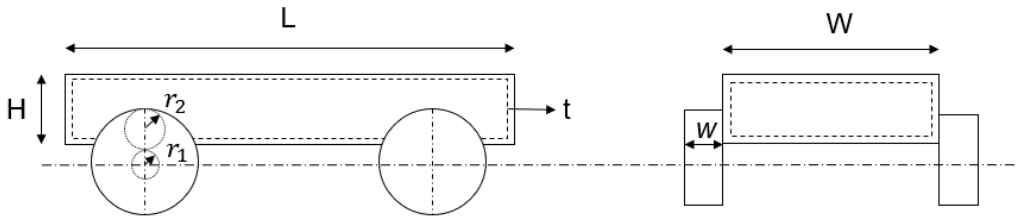

Figure 4. *Variables of the chassis*

Similarly, the dimensions of the wheel are considered as variables as their minimum and maximum allowable values are known but optimization helps to pinpoint

where the optimal values converge. The wheel width can be taken as a variable or a parameter. Since, a large wheel width adds weight significantly while low wheel width makes the robot unstable, an intermediate number is selected. However, post optimality analysis is carried out to determine the effect of wheel width on the objective space to justify considering it as a parameter rather than a variable. The payload on the robot is a fixed value as the weights of all the sensors and motors are known. Similarly, materials used for construction of the chassis are limited and do not warrant for the density to be a variable.

3.2 Assumptions

The objective function cannot be formulated unless some assumptions are made in terms of the chassis and the behavior of the robot. The assumptions are stated below:

1) Chassis is a hollow rectangular solid.
2) The maximum height of the stair that robot can climb is 200 mm [41].
3) Density of the materials used is known.
4) The payload on the robot is 6 kg.
5) The wheel width is 30 mm.
6) The center of gravity (CG) of the robot lies exactly in the middle of the chassis.
7) The gear ratio between central and partial gear is one.

The chassis of the robot is considered to be rectangular hollow box for modeling as most of the UGVs have similar shape. The height of the stair is determined based on the common staircase construction standards. The density of the material used for the

chassis is not taken as a variable as materials are somewhat limited for construction and thus, is reasonable to consider it as a parameter rather than a variable as explained earlier. Similarly, the payload and wheel width are considered fixed at this stage of optimization. The payload is estimated by adding the weight of the four motors (around 2kg), weight of the batteries (~2kg) and all the other electronic circuitry and sensors (~2kg). These assumptions are based on the commercially available motors, batteries, and sensors. More information about the embedded payload is detailed in Chapter VIII. The CG (which will be later optimized) is set in the middle of the robot and the gear ratio is set to one for simplicity.

3.3 Objective

The objective of this optimization is to reduce the torque required to climb the stairs. This also results in minimization of the robot weight. The torque is expressed as the effort required by the robot to climb a stair with a moment arm measured from its CG up to the tip of its leg. This is calculated by determining the weight of the robot with its chassis dimensions as chassis variables and wheel dimensions as wheel variables. The weight of the robot is the sum of the weight of the rear wheels, the estimated payload, and the weight of the chassis. This is reasonable as the front wheels will be lifting the entire chassis and rear wheels as they hit the stair or an obstacle. The distance from the tip of the leg to the center of the central gear is based on an empirical relation [34]. The torque required to lift the robot is equal to the gravitational pull of the robot acting at its CG.

Since, torque required on a single wheel is needed the gravitational force is divided by a factor of 2. This boils down to the following objective function:

$(L, W, H, t, r_1, r_2) \rightarrow$

$$\tau = \left({}^{g}/_{2}\right)\left(L/2 + 2.42(r_1 + r_2)\right)\left(2\pi w\rho(r_1 + 2r_2)^2 + \rho\left(LWH - (L - 2t)(W - 2t)(H - 2t)\right) + P\right) \quad (0\text{-}1)$$

The objective function in **(0-1)** can also be expressed in form of a 6-by-1 vector ***x*** which is given by

$$\begin{aligned}\tau = \left({}^{g}/_{2}\right)&\left(x(1)/2 + 2.42(x(5) + x(6))\right)\left(2\pi w\rho(x(5) + 2x(6))^2\right. \\ &+ \rho\big(x(1)x(2)x(3) \\ &- (x(1) - 2x(4))(x(2) - 2x(4))(x(3) - 2x(4))\big) \\ &\left. + P\right)\end{aligned} \quad (0\text{-}2)$$

3.4 Constraints

The Multidisciplinary Optimization involves adding constraints on the objective function to optimize the variables. These constraints include the following:

1) Upper and lower bounds on variables
2) Linear equality constraints
3) Non-linear equality constraints
4) Linear inequality constraints
5) Non-linear inequality constraints

The first type of constraints is determined by looking at the current UGV dimensions for the variables associated with the chassis, while the radii of wheel depend on the maximum height the robot should be able to climb. Upper and lower bounds on

each variable are given in **Table 9.** The LB represents the lower bound while UB denotes upper bounds. All the values are in millimeters.

Table 9. *Variable bounds*

No	Variable	LB	UB
1	Length of the Chassis	400	700
2	Width of the Chassis	300	600
3	Height of the Chassis	70	100
4	Thickness of the Chassis Wall	5	10
5	Radius of the Central Gear	32	43.2
6	Radius of the Partial Gear	21.6	32

Linear equality constraint defines the gear ratio between the last two variables i.e. the radii of central and partial gears. This can be altered as needed. However, it has been set to unity for the current optimization. No non-linear equality constraints are considered. Linear inequality constraints are listed below.

- **Ratio between wheelbase and track:** The wheelbase can be defined as the distance between front wheel and rear wheel while track is the distance between front wheels or rear wheels. According to the standard code used to manufacture vehicles, a range of 1.4-1.7 is desirable for most of the vehicles based on the drag while moving, sharp turning and other space constraints. Since the speed of the robot is considerably low, a range of 1.2-1.5 is considered to minimize the weight but to also have stability. Thus, this constraint is expressed as:

$$1.2 < \frac{L}{W} < 1.5$$

- **Rollover tendency:** Since the robot needs to turn frequently to exhibit the passive actuation, it is important to consider its stability while turning to avoid rollover. The standard rollover ratio is given by the *SSF* (Static Stability Factor). The SSF can be given as follows:

$$SSF = \frac{W}{2 \times h}$$

$$SSF = \frac{W}{2 \times 2.86 \times 2.42(r_1 + r_2)/2}$$

$$1.3 < SSF < 1.5$$

where h is the height of the center of the gravity from the floor. It is calculated from maximum height climbing capability with a gear ratio of unity from the obstacle height and the radii of the gears.

A constraint regarding the maximum allowable deflection on the chassis is considered as a non-linear inequality constraint. It is important for the chassis to not bend over time due to its own weight and payload as it can affect its climbing capabilities drastically. Currently, as the CG lies in the middle of the chassis, a structure of a simple supported beam is assumed with the point load acting in the middle of the beam. Thus, this inequality constraint is given as

$$\delta = \frac{PgL^3}{3EI} < 1\ mm$$

where E is the modulus of elasticity (238 GPa for Aluminium) and I is the moment of inertia calculated by

$$I = \frac{WH^3 - (W - 2t)(H - 2t)^3}{12}$$

3.5 Results and Discussion

The results from the optimization are summarized in **Table 10**. The results are obtained from the steepest gradient descent algorithm used in Chapter II. The algorithm uses an iterative process to take a step along the maximum slope to reach a local minimum in the objective space. The results are generated by using MATLAB.

The top half of the table provides the value of each variable after optimization while the bottom half shows the value of the torque and weight after substituting the optimal values of the variable in the optimization function. The length and width of chassis converge to intermediate points in their ranges due to various contradictory constraints. However, height of the chassis, thickness of the walls and radii of wheels converge to their lower bounds as there are no constraints that require them to be of a higher value. It is obvious that the lowest values clearly reduce the torque and thus convergence towards the lowest is observed. The torque and weight values are reasonable justifying the formulation of the objective function and constraints on the variables as well.

However, it is noted that this analysis does not include the stability of the robot while climbing. It is important to locate the CG accurately as it affects the climbing capability significantly. To avoid toppling of the robot, another optimization is carried out to calculate the longitudinal and vertical position of the CG. This is shown in Chapter IV.

Table 10. *Optimal values of variables and functions*

No	Variable	Optimal Value
1	Length of the Chassis	438 mm
2	Width of the Chassis	383 mm
3	Height of the Chassis	70 mm
4	Thickness of the Chassis Wall	5 mm
5	Radius of the Central Gear	32 mm
6	Radius of the Partial Gear	32 mm
	Functions	
1	Torque	17.58 Nm
2	Weight	10.97g

CHAPTER IV

OPTIMIZATION AND ANALYSIS OF CENTER OF GRAVITY

As mentioned in Chapter III, it is essential to locate the CG accurately for the robot to be able to climb stairs successfully. The first step is to develop a function that will be able to estimate the gradient of the robot ascent. Dynamical analysis of the robot is carried out to derive equations of motion. Once the function is defined, the optimization is conducted to maximize the ascent of robot. It is essential to find out the maximum limit of slope that the robot can overcome without turning over.

4.1 Conditions

Figure 5 shows the dynamics involved. There are two main conditions involved to locate the position of CG. The first condition is when the CG is in the middle of the vehicle and the second condition is when its longitudinal position is undetermined. The length of the vehicle (*L)* and the height of the CG/ COM from the ground is measured in *mm*. the mass of the vehicle (*m*) is in *kg* while, the frictional force (*F*) is in newtons (N). The slope (β) is in degrees and the coefficient of kinetic friction is denoted by μ.

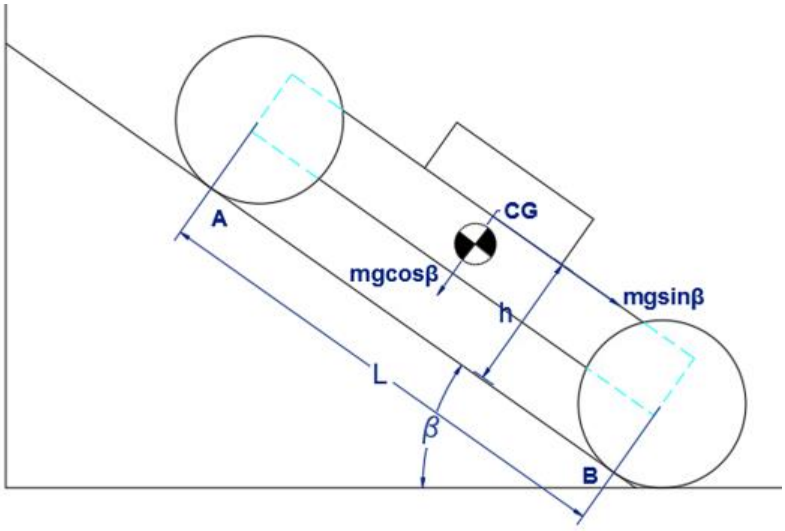

Figure 5. *Dynamic analysis of CG*

Case I: Overturning of the vehicle when CG is at the center

$$\sum M_B = 0$$

$$mgh \sin\beta = 0.5mgL \cos\beta$$

$$\therefore \beta = \tan^{-1}\left(\frac{L}{2h}\right) \quad \text{(0-1)}$$

By inserting L= 483 mm and h= 70 mm (in wheeled mode) in **(0-1)**, the value of the gradient is found at around 74°. The value of the length is taken from the Chapter III which gave the optimal value as 483mm. The value of the height of the CG is assumed to be approximately at the radius of the wheel. This gives the value of 70mm. As the motors will be below the chassis and other circuitry above the chassis this is a reasonable assumption. When the wheels turn into legged mode however, the CG raises to a value of around 150mm. This is based on an empirical relation [34], which gives the distance

between the tip of the leg to the center of the central gear. In this case, with L= 483 mm and h= 150 mm (in legged mode), the gradient is around 58°.

The gradient reduces significantly as the robot changes its mode to legged mode as the CG goes higher. This gradient is however acceptable as staircases do not have slopes larger than 50° [41]. This is not a sufficient margin for safety. On optimization, the lower limit on the height of the CG and the upper limit on the length of the vehicle is obtained. This warrants to another optimization which will involve the objective of Chapter III as well as the objective in this chapter. Another case studies the effect of having the CG slightly in front of the vehicle rather than in the middle of the vehicle. This case is explained below.

Case II: Overturning of the vehicle when CG is near the front wheels

$$\beta = \tan^{-1}\left(\frac{L}{h}.x\right) \tag{0-2}$$

where the value of x is the fraction of the position of the CG along the length of the robot measured from point B. For example, when CG is in the middle of the vehicle value of x will be 0.5 which means that it is at $0.5L$. The value of x can be found out by optimization. Having a higher x is beneficial as it gives a higher slope.

4.2 Objective

The objective of this optimization is to maximize the slope of the robot ascent. This means that the maximum slope which the robot will be able to climb securely. The variables involved in the optimization are L, h, and x. The objective function is β, as given by **(0-2)**.

4.3 Constraints

There are only upper and lower bound constraints involved in this optimization. The length of the chassis has the same bounds as in Chapter III. The height of the CG varies from 20mm to 200mm as explained earlier. While, the fraction of CG varies from 0.5 to 1. Having the fraction closer to unity helps to have maximum slope but maintaining the CG near the front is not possible due to space constraints. Also, it is yet unknown as to how that affects the torque required to climb as this objective is independent of the objective from Chapter III.

4.4 Results

The steepest gradient descent optimization is carried out to determine the optimal values of the variables. The length converges to its upper bound as expected while the fraction of longitudinal position of CG and the height of the center of the gravity converge to their upper bounds as that will make the slope highest. However, this does not show how each variable affects the objective function. That can be done by plotting each variable in the objective space.

4.5 Graphical Analysis of CG

Graphical analysis can help determine the relations between the three variables involved in the optimization, namely, *L*, *h*, and *x* and the objective function which is β.

First, the effect of *h* on the objective function is determined. **Figure 6** shows how the height of CG affects the slope. When the CG is lower, the robot can climb steeper slopes but as the height increases the slope decreases. Having the height between 70mm to 200mm will give a substantial margin of safety.

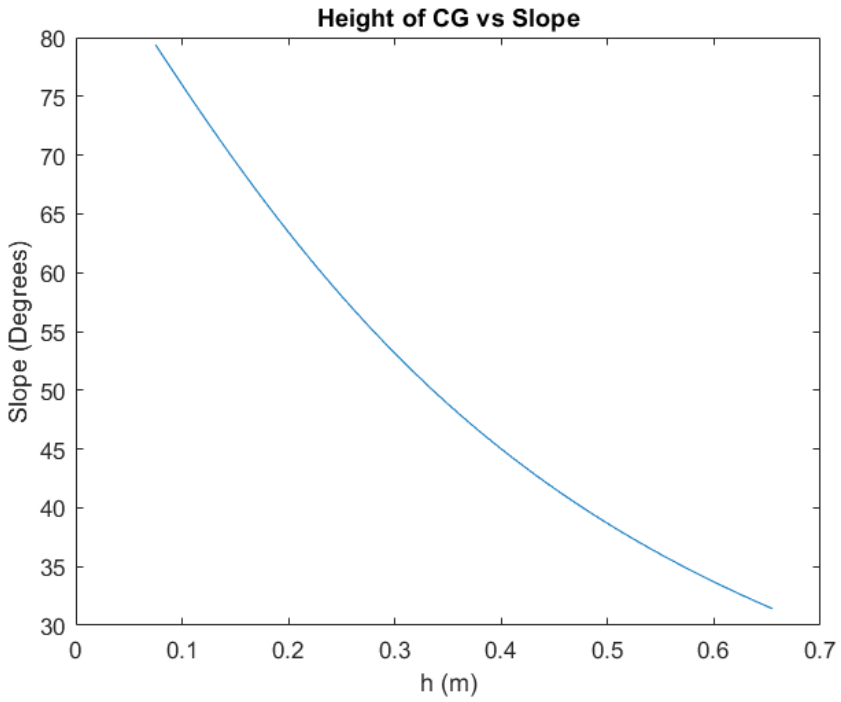

Figure 6. *Effect of height of CG on slope*

Figure 7 shows how the slope decreases as the CG is moved backwards. This gives a relation between the objective function with respect to **x**. Even though the change does not seem significant, it allows to increase the margin of safety while not having to change

or modify any factors involved in chassis design. It can be seen that if the value of ***x*** is to be kept 0.55 to 0.67, the slope increases as compared to having it in the middle at 0.5.

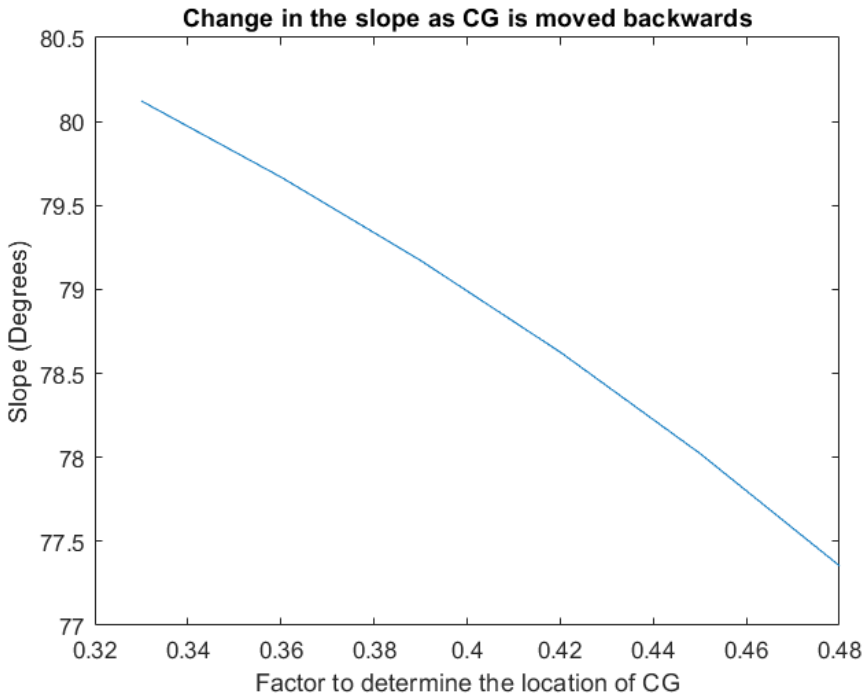

Figure 7. *Effect of longitudinal position of CG on slope*

Figure 8 shows the relation between length of the chassis and the slope. It is obvious that having a longer chassis will help the robot to climb higher slopes but after 600mm the slope flattens and thus, that is taken as an upper bound on length of the chassis.

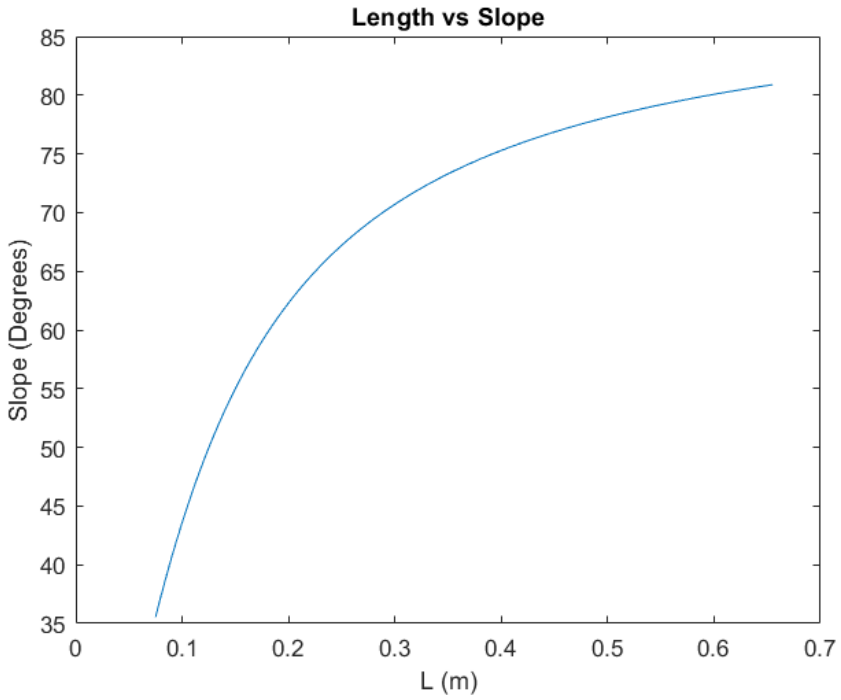

Figure 8. *Effect of length of chassis on slope*

It is essential to find an optimal trade-off between the maximum slope that the robot can travel versus the minimum torque which it requires to climb an obstacle. It is important to look at both objectives from Chapter III and Chapter IV together to have an optimal solution. Thus, Chapter V deals with a Multi-objective optimization to optimize the 2-D objective space by the method of Pareto Front.

CHAPTER V

MULTI-OBJECTIVE OPTIMIZATION

Often while optimizing complicated mechanical systems, there are contradictory objectives involved. The optimal values provided after optimization of the first objective may cause adverse effects to the value of the second objective. It is necessary to find a set of solutions that may not be the most optimal set for each individual objective but is one for the combined objective space. This is explained in this chapter by the method of Pareto Front.

5.1 Objectives

The robot should be able to climb the maximum possible slope without turning over while at the same time should require the minimum possible torque to do that.

- Objective 1: Maximization of the robot ascent.
- Objective 2: Minimization of the torque required to climb the stairs.

The combined objective space has following variables (**Table 11**) and parameters (**Table 12**).

Table 11. *List of variables*

No	Variable	Symbol	Representation
1	Length of the Chassis	L	*x(1)*
2	Width of the Chassis	W	*x(2)*
3	Height of the Chassis	H	*x(3)*
4	Thickness of the Chassis Wall	t	*x(4)*
5	Radius of the Central Gear	r_1	*x(5)*
6	Radius of the Partial Gear	r_2	*x(6)*
7	Longitudinal Position of CG	L_{CG}	*x(7)*
8	Vertical Position of CG	V_{CG}	*x(8)*

Table 12. *List of parameters*

No	Parameter	Symbol
1	Wheel Width	w
2	Density of the Chassis Material	ρ
3	Payload	P

Let us consider the objective space to be a vector $\boldsymbol{z} \in \mathbb{R}^2$, each row containing a single objective function. This can be re-written in form of the variables as follows:

$$\boldsymbol{z} = \begin{bmatrix} z(1) \\ z(2) \end{bmatrix}$$

where

$$z(1) = -\tan^{-1}\left(\frac{x(1) \times x(7)}{x(8)}\right) \tag{0-1}$$

$$\begin{aligned} z(2) = (g/2)\big(x(1)/2 + 2.42(r_1 + r_2)\big)\Big(2w\rho\pi(r_1 + 2r_2)^2 \\ + \rho\Big(x(1)x(2)x(3) \\ - \big(x(1) - 2x(4)\big)\big(x(2) - 2x(4)\big)\big(x(3) - 2x(4)\big)\Big) + P\Big) \end{aligned} \tag{0-2}$$

The negative sign in **(0-1)** indicates that it needs to be maximized. The Pareto Front algorithm considers the objective space to be minimized. Both objectives in **(0-1)** and **(0-2)** are identical to those found in Chapter III and Chapter IV.

5.2 Scaling of Objectives

As shown in the objectives, the first objective outputs an angle in degrees or radians while the second objective gives the value of torque in newton meters. Since these objectives have different units, there is no way to compare them together by the optimization without modification. The optimization done this way will result in poor accuracy. Scaling of the objective space can be done by normalization process. For the first objective, the function is divided by its maximum value. Similarly, for the second objective, the function is divided by the maximum torque. This way, both *z*(1) and *z*(2) lie in a space from 0 to 1. Furthermore, each objective function can be given a weightage. In this case it is more important to have lesser torque than to have the robot climb higher slopes as most of the staircases do not run at maximum slope. Therefore, the weight

assigned to the first objective function is 0.6. This means that, it is 40% less important than the second objective.

The optimization will now put a higher preference to the second objective function in **(0-2)**. The updated ***z*** is given by **(0-3)** and **(0-4)**.

$$z(1) = (f_1)\frac{-\tan^{-1}\left(\frac{x(1)\times x(7)}{x(8)}\right)}{z_{1_{max}}} \tag{0-3}$$

$$\begin{aligned} z(2) = (f_2)(g/2)\big(x(1)/2 \\ + 2.42(r_1 + r_2)\big)\Big(2\pi\rho w(r_1 + 2r_2)^2 \\ + \rho\Big(x(1)x(2)x(3) \\ - \big(x(1) - 2x(4)\big)\big(x(2) - 2x(4)\big)(x(3) \\ - 2x(4))\Big) + P\Big)/z_{2_{max}} \end{aligned} \tag{0-4}$$

where $f_1$is weight factor for $z(1)$, f_2 is weight factor for $z(2)$, $z_{1_{max}}$ is normalizing factor for $z(1)$ and $z_{2_{max}}$ is normalizing factor for $z(2)$.

5.3 Constraints

The constraints on the objectives are same as seen in Chapter III and Chapter IV. This chapter combines the two hence, they remain same. **Table 13** shows that there are no changes in the upper and lower bounds of the variables apart from the addition of the last two variables and their bounds in case of multi-objective optimization.

Table 13. *Bounds on variables*

No	Variable	LB	UB
1	L	400 mm	700 mm
2	W	300 mm	600 mm
3	H	70 mm	100 mm
4	t	5 mm	10 mm
5	r_1	32 mm	43.2 mm
6	r_2	21.6 mm	32 mm
7	L_{CG}	0.5	0.75
8	V_{CG}	70 mm	200 mm

The linear equality constraints are same as in Chapter III. The linear inequality constraints of the rollover tendency and the ratio between wheel and track remain unchanged. There are no non-linear inequality constraints. The non-linear equality constraint still applies the limitation on the maximum deflection permissible on the chassis. Now that the position of the CG is not fixed longitudinally, this constraint changes to a problem of a simply supported beam with point load applied away from the center.

$$\delta = \frac{Pga^2(L-a)^2}{3EIL} < 1\ mm$$

where a is the distance of CG from the left end (i.e., $a = L_{CG}.L$), and I=$\{WH^3 - (W-2t) \times (H-2t)^3\}/12)$. The optimization is then carried out by the method of Pareto Front and the plot generated can be seen in **Figure 9** by using MATLAB.

5.4 Analysis of Pareto Front

The parameters associated with the Pareto Search algorithm are written in **Table 14**. The default constraint tolerance is enough for the objectives to be constrained sufficiently tight. The maximum number of iterations and Pareto set size has been increased to span the objective space better than the default values. The computation time is not affected due to these changes.

Table 14. *List of parameters of Pareto Front*

No	Parameter	Default Value	Current Value
1	Constraint tolerance	10^{-6}	10^{-6}
2	Maximum iterations	1000	5000
3	Pareto set size	60	200

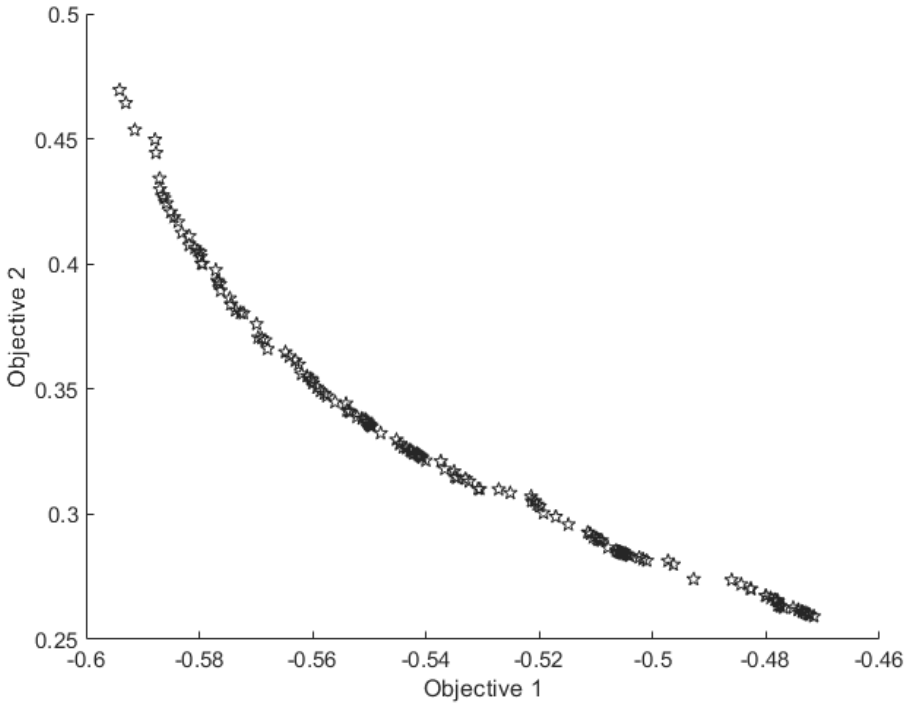

Figure 9. *Pareto Front of the objective space*

5.4.1 Observations

There are no large gaps or unexplored areas in the Pareto Front which does not warrant to apply advanced techniques to explore the blank areas. If there are blank spaces on the front, additional mathematical modeling is performed to produce a set of points in that area. These fronts along with the original front are then used to acquire the complete set of optimal points. Since, this is not required for the current objective space, an optimal set which suits the practical considerations in manufacturing the chassis is selected from the 200 points given above. The selection of the point is completely based on designer.

5.4.2 Results

The results of the optimization can be seen in **Table 15**. This set of point is selected as it occurs in the set of 200 points most frequently with minimal changes in L and L_{CG}.

Table 15. *Optimal values of variables*

No	Variable	Optimal Value
1	L	593.4 mm
2	W	442.8 mm
3	H	80 mm
4	t	5 mm
5	r_1	32 mm
6	r_2	32 mm
7	L_{CG}	0.67
8	V_{CG}	70 mm

5.5 Interpretations of the Results

The results obtained from the optimization are interpreted as follows:

- L: The length is converged to a point between its lower bound and upper bound. The length must be lower to minimize the torque but not as low as its lower bound to conform to the wheelbase to track ratio. However, having longer chassis enables the robot to climb steeper slopes. Thus, due to these contradictory objectives and constraints it settles at an intermediate point rather than its bounds.
- W: The width is directly affected by length because of the linear inequality constraint as mentioned above and is also used to determine the rollover tendency. Therefore, it converges to an intermediate point in its range like the length.
- L_{CG}: This variable needs to be as large as possible to minimize the torque and maximize the ascent but it is also restricted by the maximum allowable deflection which brings it closer to the lower bound but not converge to it. This is measured from the rear of the vehicle.
- As seen from the table the rest of the variables converge to their lower bounds. This is expected as they are not involved in contradictory constraints and all of them optimize both objectives by being at their lowest values.

Now, it is important to find out the effects of these variables on the objectives as well as the effects of the fixed parameters on the objective functions. This can be achieved by post-optimality analysis. This is a statistical technique to quantify the effects of not only variables, and parameters but also constraints, on the objective space. The components in the analysis are described in Chapter VI.

CHAPTER VI

POST OPTIMALITY ANALYSIS

This chapter deals with the post processing of an optimization algorithm. The post processing helps a designer to understand the importance of each variable on the objective space. It tells the designer how each variable affects the objective space and how changing its value changes the objective function. This analysis also provides justification of pre-determination of parameters such as the density of chassis material, payload, and wheel width. It allows one to know how a different material with different density affects the objective and whether that parameter can be changed flexibly or whether it has a significant effect on the objective function. Moreover, it also gives insights into the constraint flexibility. There are four steps involved in this analysis. The steps are as follows: 1) scaling, 2) constraint sensitivity analysis, 3) variable sensitivity analysis, and 4) parameter sensitivity analysis.

6.1 Scaling

This process involves normalizing the objective functions and the variables to allow them to lie in a comparable dimensionless space.

6.1.1 Scaling of Objective Functions

The scaling of the objective function in multi-objective optimization is important since a large difference of magnitude between two objective functions can affect the

optimal solution. A standardized way to scale the objective functions is to divide them with their maximums. This would ensure both the objectives spanning the space of zero to one. The maximum values can be obtained by carrying out the optimization of the same objective function but with its sign reversed. The scaling is already performed while conducting Pareto Front optimization as explained in Section 5.2 of Chapter V.

6.1.2 Scaling of Variables

The scaling of the variables is an important aspect in real life engineering problems as the units and magnitudes differ greatly and sometimes it can result in less than the optimal outputs. There are various methods to identify the need of scaling, but the most popular way is by determination of the Hessian Matrix of the objective function. It is important to scale the variables when the Hessian is *ill-conditioned*.

The Hessian gives the second derivatives with respect to each variable and is used to locate the critical points, i.e. Maxima, minima and saddle points. The analysis can be easily carried out in case of a lesser ordered Hessian. Since the objective space has a 8×8 Hessian it is better to use the method of Diagonal Scaling of Variables. This involves considering only the diagonal entries on the Hessian. If the diagonal entry is between the magnitudes of 10^{-2} and 10^{2} then there is no need for scaling. All the variables in the objective function lie in this range except for the sixth variable which is the wall thickness of the chassis. The scaling is carried out for x_6 as follows:

$x_6 = x_6 \times 10^{-2}$. This allows all the diagonal entries of the Hessian to be in the allowable range. Then the optimization is carried out with the modified objective function.

The results however come out to be the same, so the results of the scaling remain inconclusive. An optimization process by scaling of variables does not always provide conclusive results as it is not always possible to mathematically model the entire mechanical system fully.

6.2 Sensitivity of Constraints

After the optimization it is important to find out the active and inactive constraints. If the Lagrange Multiplier of a constraint is non-zero at the optimal vector then, the constraint is said to be active. An active constraint indicates that at the optimal output that constraint is keeping the variables and the objective in the bounds. An active constraint will change the objective function when the constraint tolerance is increased. Thus, this analysis helps to determine which constraint should be given more importance and which constraint should be of lower preference. **Table 16** shows the dominant constraints and their effects on the objective space. Each value in a cell gives the percentage change in the objective when that particular constraint is made stricter by 10% or made more tolerable by 10%. For example, if the lower bound of length is increased by 10%, the objective function increases by 13% which is significant. However, if the linear equality constraint seen in Chapter V is decreased by 10% it has negligible effect on the objective function.

Table 16. *Sensitivity analysis of constraints*. *LE- Linear Equality; NLIN- Non-linear Inequality; LB- Lower bounds*

	Change in the Torque	
Constraint	**Increment by 10%**	**Decrement by 10%**
LE	-1.20%	1.50%
NLIN	-0.14%	0.19%
LB *L*	13%	-10%
LB *B*	4.70%	-1.70%
LB r_2	2.90%	-0.14%
LB *t*	12.50%	-2.10%

Observations

- If the lower bound of the length is increased the output increases significantly and if it is lowered a better minimization can be achieved.
- If the lower bound of the wall thickness is increased the output will increase significantly. However, decreasing the wall bound does not change the output appreciably.
- The rest of the constraints do not have a significant impact.

This analysis helps figuring out which constraints are most sensitive and allows the designer to be wary of changing them as they change the objective function drastically.

6.3 Sensitivity of Variables

The analysis of variable sensitivity gives an idea of the effect of change in the value of the variable on the objective functions. The most sensitive variables should be handled with precaution and the least sensitive can be flexible with respect to their bounds and constraints. The tornado chart shown in **Figure 10** displays the sensitivity of each variable. Each variable is normalized in a dimensionless space to allow comparison between them. The normalization procedure is carried out as given in Chapter II. Since, the objective space is bigger the calculations are performed in MATLAB.

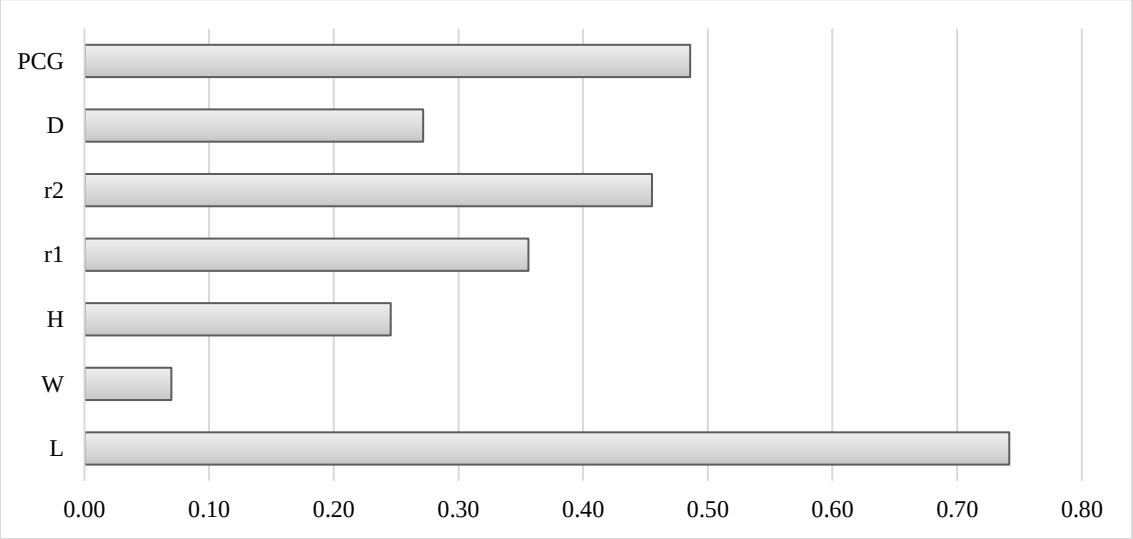

Figure 10. *Sensitivity analysis of variables*

Interpretations

L is the most sensitive parameter in the design of the platform as a slight change in its value will affect the performance of the robot drastically. A longer chassis will be more stable. Moreover, changing the L_{CG} will reduce the climbing capability. Keeping it at the rear end will make the vehicle topple while climbing but keeping it slightly in the front will improve not only the ascent but also descent of the robot on stairs. The change in r_2 is also significant as it will affect the torque required to climb the stairs. Rest of the variables are not as sensitive and can have some flexibility while manufacturing.

6.4 Sensitivity of Parameters

The parameters in an optimization problem are the fixed values which are pre-determined such as the density of the material used for chassis ρ, payload on the robot P and width of the wheels w. The sensitivity of these parameters is shown in **Figure 11**.

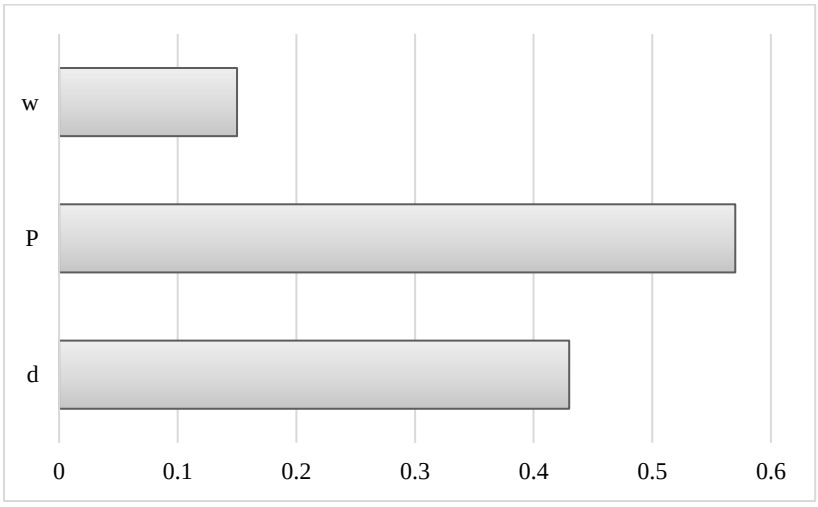

Figure 11. *Sensitivity analysis of parameters*

Interpretations

Increasing the values of P and ρ will result in significant weight increment which is expected. However, w has negligible effect on the performance of the robot. This justifies the fact that wheel width can be taken as a parameter rather than a variable.

The post-optimality analysis completes the process of optimization by opening an avenue to modify the variables, parameters, or constraints according to their dominance on the objective space. It helps to determine the flexibility in changing a particular value in the optimization. Once the weight of the robot increases it is important to not only optimize the chassis dimensions but also devise a method to absorb vibrations due to impact forces. This is shown in Chapter VII.

CHAPTER VII

SUSPENSION SYSTEM DESIGN

This chapter develops a spring-loaded suspension system to reduce the vibrations produced due to the robot hitting the ground in legged mode. The presented suspension system consists of torsional springs added to each leg to absorb the impact when it hits the ground. It offers following advantages:

- Mechanical simplicity: Traditional spring-damper suspension systems offer great isolation, however, tend to be mechanically complex and require additional control. This suspension system, consisting only of torsional springs is easy to install and reduces the vibrations significantly.
- Negligible weight: Since weight is one of the major factors for stair climbing robot, it is essential to have a system which does not add to the weight of the robot while attenuating the shock it endures. The springs add negligible weight to the robot.
- Terrain adaptability: Having torsional springs help robot to close its legs due to the spring energy which is desirable in a terrain where the robot does not need to have its legs opened, resulting in a faster speed.

The design of spring presented in this chapter is based on failure analysis [39].

7.1 Design Principle and Assumptions

The strain energy stored in the spring due to the bending moment is integrated over the entire length of the spring with active coils to find out the stiffness and other parameters. The assumptions involved in the design of spring are listed below.

1) The operating torque is 10% of the stall torque
2) The force acting on the spring is equal to the force with which the leg hits the ground or an obstacle
3) The losses in the geared mechanism are considered to calculate the final moment(M_b) acting on the spring
4) The Grade of the spring is taken as 3, which indicates the design would be subjected to moderate to severe stresses.
5) The yield strength of steel (S_{yt}) is 60% of the ultimate tensile strength(S_{ut})
6) The factor of safety (fs) is taken as 1.5.

7.2 Design Process

The process involves considering a wire diameter and outer diameter of the spring and then finding out whether the selected dimensions result in failure. If they fail, next set of dimensions is chosen until the allowable stresses are less than the failure stresses.

Initially, the moment subjected to the spring is calculated. In this case, it is the moment calculated by impact force produced as the leg hits against the ground with respect to the center of the central gear. Then, the material and a set of dimensions of the spring are selected for the first trial. The spring index is the ratio between the outer diameter of

the spring and the wire diameter. Wahl factor is a factor developed to calculate the torsional shear stress, direct shear stress and stress produced due to the curvature in the spring. The maximum allowable stress on the spring is calculated with help of ultimate tensile strength and yield strength of the spring. The actual bending stress on the spring must be less than this. This stress is determined by using the first set of dimensions and moment calculated earlier. All these factors are calculated as shown in ***(0-1)***. If this stress is less than the allowable stress, the design is considered to be safe. However, if it is higher than the allowable stress, a second set with higher dimensions is chosen and the entire process is repeated until the stress is less than the permissible stress by a sufficient margin. The flow of the steps is shown in **Figure 12**.

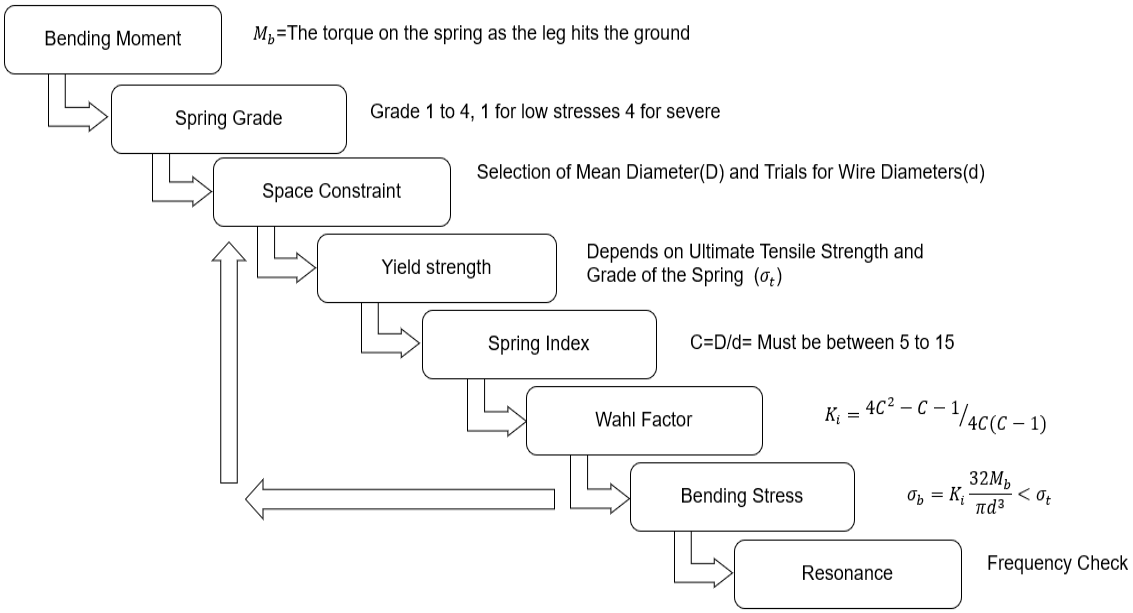

Figure 12. *Steps in spring design*

The wire diameter of the spring is given by d and the outer diameter of the spring is given by D. Permissible stress (σ_t), spring index (C), Wahl's factor for the inner diameter (K_i), and the bending stress (σ_b) are calculated as below:

$$\sigma_t = \frac{S_{ut}}{fs} = \frac{0.6 \times S_{yt}}{fs};\ C = \frac{D}{d};\ K_i = \frac{(4C^2 - C - 1)}{4C(C-1)};\ \sigma_b = K_i\left(\frac{32M_b}{\pi d^3}\right) \qquad (0\text{-}1)$$

Table 17 displays the results from the "trial-and-error" method to determine spring parameters. The first two columns are the dimensions selected prior to the trial. Next four columns are calculated based on **(0-1)**. The last column compares the value of σ_b and σ_t. If the value of σ_b is less than the value of σ_t, the design is safe as the stress subjected on the spring is less than the permissible stress.

Table 17. *Trials in spring design*

Trial	D (mm)	d (mm)	C	K_i	σ_t $(\frac{N}{mm^2})$	σ_b $(\frac{N}{mm^2})$	Result
1	10	1	10	1.08	896	6603.8	Not safe
2	10	1.4	7.14	1.11	836	2488.67	Not safe
3	12	1.6	7.5	1.11	832	1656	Not safe
4	12	2	6	1.14	796	872	Not safe
5	16	2	8	1.1	796	832	Not safe
6	18.9	2.16	8.75	1.09	796	667	Safe

Based on the above trials, a spring with wire diameter bigger than 2 mm and outer diameter upwards of 16 mm is a safe option. From the manufacturer's catalogue a spring is selected whose wire diameter is 2.16mm and outer diameter 18.9mm.

Resonance:

Operating frequency is taken to be the rotational speed of motor. The natural frequency of the spring is much higher than the operating frequency.

7.3 CAD and Manufacturing

Once the springs are selected, modifications are made on the wheel design for spring installation. This design is compact and secure. The exploded view of the assembly of the suspension system is shown in **Figure 13** (left) and **Figure 13** (right) shows a close view of the torsional spring mounted around the spoke frame in a cavity on the partial gear. The torsional spring has one end activated by the impact sustained by the leg upon collision and the other end is supported by the modified design of the spoke frame. The suspension system is tested to determine its locomotion performance and compare with a version without suspension.

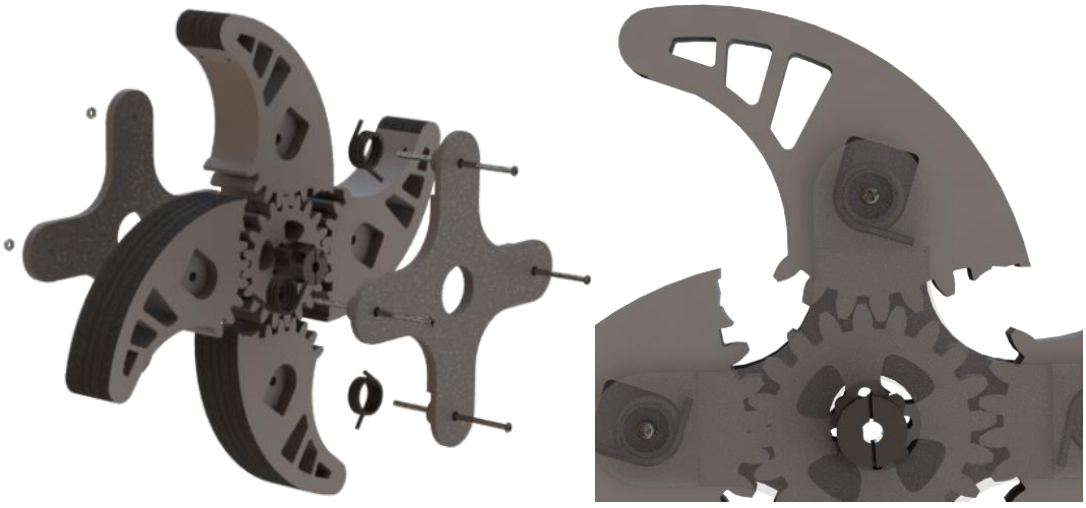

Figure 13. *CAD of the exploded view of the assembly (left) and close-up view of the spring (right)*

Figure 14. *Fully assembled spring-loaded wheel with 3-legs (left) and 4-legs (right)*

Figure 14 shows WheeLeR in 3-leg and 4-leg configurations equipped with the proposed spring suspension system. As shown in the figure, this suspension system is suitable for different wheel configurations while one with a large number of legs will have a relatively small size leg segments, making it hard to fit the spring with the desired properties.

7.4 Testing and Evaluation

The performance of suspension system is evaluated by an onboard IMU on Pixhawk Orange Cube. The tests are carried out for wheels with suspension and without suspension in legged mode, outdoors and for 30 seconds each. The Pixhawk uses an embedded algorithm to calculate the vibrations [42]. The raw values from accelerometer are filtered by a high pass filter to create a reference set and standard deviation of the latest value of vibration is determined with respect to the reference which again, is filtered to

give the final output. The results obtained along each direction are shown in **Table 18**. The last column shows the decrease in the vibrations due to the spring suspension system.

Table 18. *Magnitudes of vibrations along three axes*

Direction of Vibration	With Suspension	Without Suspension	% Decrease
x	5.04	6.68	26
y	5.2	7.13	27
z	**6.03**	**10.47**	**42**

As shown in **Table 18**, adding the suspension system reduces the vibrations significantly. The vibrations in vertical direction are along *z*-axis and are most dominant vibrations. These are damped up to 40% which will reduce the shocks considerably. The vibrations along *x* and *y* directions are also dampened by 26% and 27%, respectively. Therefore, adding a suspension system not only absorbs impacts but also provides a smoother walking performance.

Once the wheels are equipped with the suspensions system, the next step is to design a chassis, manufacture it as per the suggested dimensions, and configure the sensors to complete the hardware of the robot. This is described in Chapter VIII.

CHAPTER VIII

SENSOR CONFIGURATION AND CHASSIS ASSEMBLY

As the dimensions of the robot are finalized and the wheel suspension system is developed, hardware design and assembly can be initiated. This chapter presents the electronic components and their assembly, sensor configurations, and hardware fabrication and assembly. For the developed robot to perform practical tasks, localization, navigation, and wireless communication are considered required technical functions. To do so, the robot must be capable of sensing its own position, detecting surroundings, and scoping out potential obstacles.

8.1 Main Processor and Embedded Sensors

8.1.1 Microcontroller

Jetson TX2 Development Board is the processing unit of the robot. It has NVIDIA's latest Pascal GPU along with twice the memory and bandwidth to that of its predecessor, Jetson TX1. It also supports almost all the communication protocols like CAN, UART, I2C and GPIOs. It has the provision to extend SMA connectors for a wider network coverage and has mini USB and USB 3.0 ports if added to the developmental board. It is the central processing unit of the robot. All the sensors are connected to it to

provide their feedback which is then processed to send appropriate signals to the drive system. The motor controller is also connected to TX2.

8.1.2 Sensors

The robot is equipped with following sensors for navigation and data collections.

- Pixhawk Orange Cube and Here3: This module comes with three IMUs consisting of triple axis accelerometers, gyroscopes, and magnetometers. The module also consists of a barometer. The Here3 is a GNSS module with global positioning capability and an IMU of its own, based on CAN protocol.

  It is powered separately by a Power Brick Mini and is connected to the Jetson TX2 through a powered USB Hub. The IMU data and GPS data is acquired through *mavros* protocol via *mavlink* using *rviz* graphical interface of ROS.
- RPLiDAR a1m8: The RPLiDAR is 360° laser scanner operated by a servo motor and can have speed control. It is used to detect obstacles and is also used in stair climbing algorithm. It is connected through the powered USB Hub to Jetson TX2. It is used in obstacle detection in *move_base* navigation.
- Intel RealSense D435i: Two of these cameras are installed, one in the front and one at the back, to generate point cloud data for the primary *move_base* algorithm for navigation. They are also used for staircase detection algorithm. The cameras are of RGB-D type capable of capturing distances up to 8 meters. One camera is connected through the USB hub while the other is connected to the Mini-USB port on TX2.

Figure 15 shows all electronic components and sensors embedded and how they are connected.

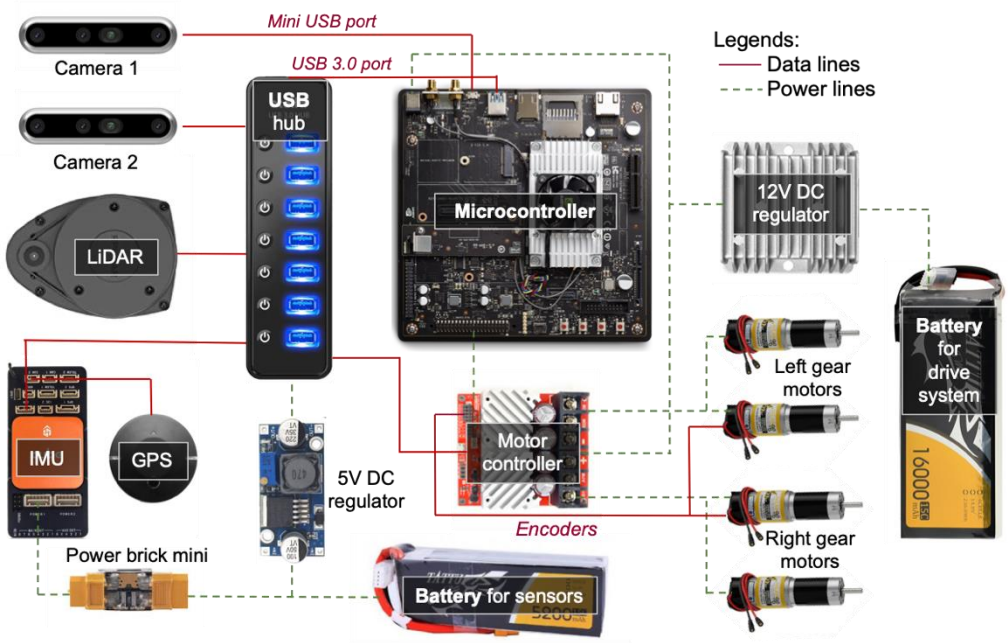

Figure 15. *Layout of the electronic components*

8.2 Drive System

The robot uses DC motors for locomotion which are controlled by a motor controller. The details of the two are listed below.

- Roboclaw motor controller: The controller is configured and calibrated through its proprietary software. Left and Right wheel encoders are attached and configured through the same. The encoders are powered through the power pins from GPIO pins of Jetson TX2. It is connected to the TX2 through USB Hub.

- Servocity Planetary Gear Motors: These DC motors have 30 RPM with 24.5 Nm stall torque. They are controlled by the Roboclaw motor controller and give encoder feedback to the controller. The motors are selected based on the torque and speed of the robot. The torque required to climb a stair of height 200mm is calculated in Chapter III. When the objectives from Chapter III and IV are combined in Chapter V, the torque obtained is about 15 Nm. The motors must provide this torque and must not be bulky or heavy as weight is a critical factor in the robot. The robot must not have too high a velocity as it may hit the stair and damage the camera or other components on impact. Moreover, while climbing up, too high a velocity may result in turning over. The speed of common UGVs is not more than 200 RPM however, torque at that speed is significantly lower. A DC motor that simultaneously satisfies the high torque demand with high speed is inherently bulky and heavy. Thus, a speed between 20-70 RPM is considered as reasonable [34]. A motor with highest torque is then chosen as it provides a margin of safety.

8.3 Power Supply

A 16000 mAh battery powers the entire drive system for the robot to be operational for at least half an hour while a separate 5200 mAh battery provides output to all the sensors and the USB hub. These are LiPo batteries which are rechargeable. The weight of the batteries is almost 2kg and hence, they are kept near the front to maintain the position of the CG near the front wheels.

8.4 Chassis Design and Assembly

The overall shape of the chassis is a hollow rectangular solid with circular contouring on the sides for weight reduction and aesthetic advantage. The materials, manufacturing processes and components are described in this section.

8.4.1 Materials

The central gears, partial gears and spoke frames are made up of PLA. This is a material that can be used for 3D printing. The infill ratio is kept at 40%. This material is durable and light, however, does not offer frictional grip. It is important for the legs to have a material with good frictional grip to maintain the transformation tendency. Therefore, a rubber sheet is attached to each leg to offer better grip as the coefficient of rolling friction affects the transition between wheel-leg mode significantly, as seen from Chapter II.

The base of the chassis is made of a carbon fiber plate. The density of carbon fiber is almost half of the aluminum hence, it cuts down the weight considerably. Although, carbon fiber is brittle, the base plate having subjected to severe stresses is highly unlikely and hence the choice is reasonable. The walls of the chassis are made of PLA, as they do not get affected by stresses and need to be as light as possible. The top cover is made of acrylic sheet which offers an appealing look along with being light in weight.

8.4.2 Fabrication

The central and partial gears are 3D printed as they have complex geometry. The spoke frames are also 3D printed as the springs need extruded seats to be installed on the spoke frame. The mounts for LiDAR, RGBD cameras and GPS are also 3D printed as they need specific geometrical fixtures. The chassis walls are 3D printed as well. The front wall and the rear wall have a window for the RGBD cameras. Two supports are added to the base plate to support the top cover. The top cover is cut by a laser cutter and the logo is engraved. The base plate is custom cut from the manufacturer as carbon fiber requires specialized machining and fabricating processes.

8.4.3 Assembly

The wheels are assembled by placing the partial gears around the central gears and installing the springs around the extrusions from spoke frames in a cavity on each leg. The other spoke frame is then bolted to the former to secure the entire structure. The motors are clamped on the base plate and wheels are connected through hubs. This way the wheels can be swapped easily. The walls of the chassis are then bolted to the base plate along with the supports for the top plate and camera mounts. All the electronic circuitry is laid on the base as shown in earlier section. The top plate is bolted to the walls along with having hinge support for easier access. The mounts of GPS and LiDAR are then bolted on the top plate to complete the assembly. The fully assembled robot can be seen in **Figure 16** and the internal design of the chassis can be seen in **Figure 17**. The stair-climbing capability of the robot with spring-loaded wheels is displayed in **Figure 18**.

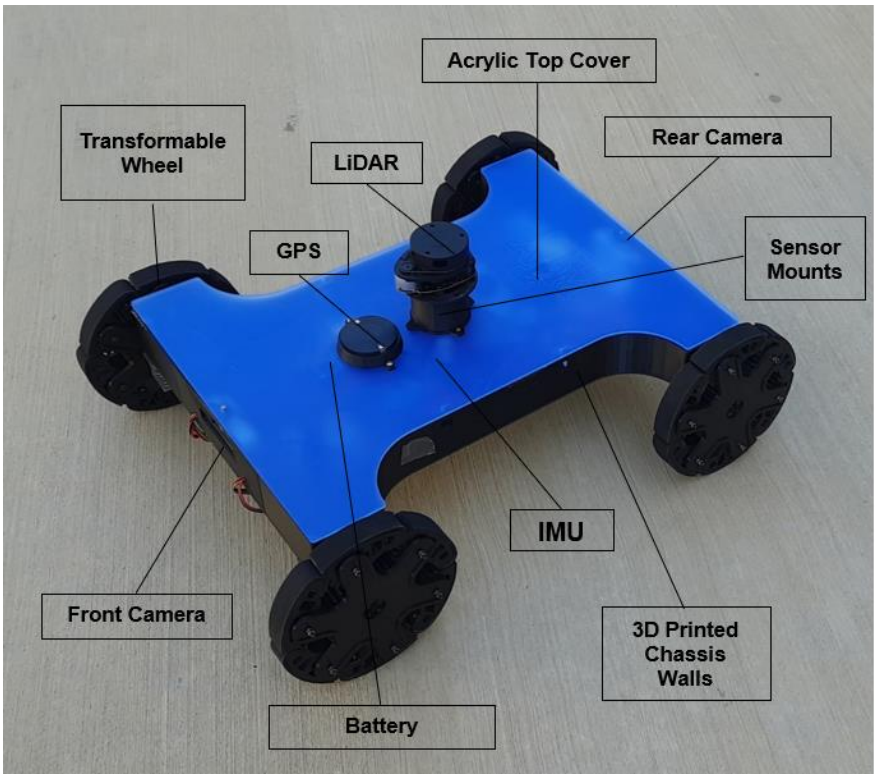

Figure 16. *Fully assembled robot*

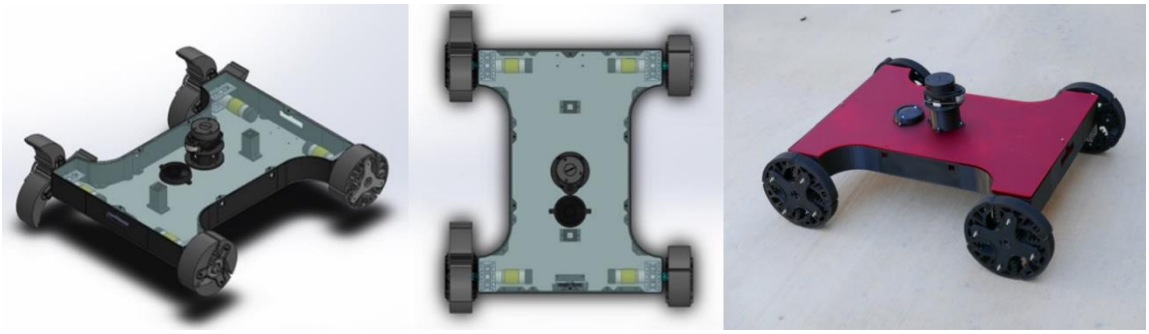

Figure 17. *CAD of the chassis (left), assembled prototype (right)*

Figure 18. *α-WaLTR climbing a staircase*

CHAPTER IX

CONCLUSION

Multidisciplinary design optimization enabled to integrate various engineering disciplines and narrowed the scope of the mechanically complex design space of α-WaLTR. The multi-objective optimization provided the best possible compromise between two contradictory objectives of minimization of the torque required to climb an obstacle and maximization of the gradient of the robot ascent. The post optimality analysis gave an insight in the effect of design variables and parameters on the objective space. It also gave an idea of the most sensitive variables, parameters and constraints which would affect the performance of α-WaLTR significantly. The analysis of the center of gravity ensured the stability of the robot while the design of a suspension system reduced the vibrations suffered by the robot. The chassis design and proper assembly of the electronic circuitry completed the hardware development to produce a platform having optimal performance.

The proposed robot can be used in numerous applications, such as emergency services in case of hazards, as it offers the unique advantages of climbing staircases. It can also be used for surveillance in diverse environments involving adverse terrains. Additionally, its versatile locomotion capability shows great potential in agricultural and farming industry. Ultimately, it can find applications in space to maneuver on unexplored surfaces.

Although the passive actuation offers unsplit advantage in terms of energy and cost reduction, there are uncertainties involved in the switching of the wheels to legged mode. It is difficult to produce, at least in a research laboratory setting, a seamless tire around the wheel which will improve the frictional grip and provide additional insulation. Additional navigation algorithms are also needed for effective wheel-leg transitional behavior. While the presented spring suspension makes the wheel more compact and modular, a standard automobile suspension system with spring and damper may be more effective than the modular torsional spring system over the course of running of the robot. Several iterations of design improvements and further development are currently being made and, with these improvements and additions, each advanced version of the robot will have more versatile and reliable climbing capabilities with robust passive actuation.

REFERENCES

[1] N. J. Nilsson, "A mobile automaton: An application of artificial intelligence techniques," *Sri International Menlo Park Ca Artificial Intelligence Center,* 1969.

[2] P. F. Muir and C. P. Neuman, "Kinematic modeling of wheeled mobile robots," *Journal of robotic systems,* vol. 4, no. 2, pp. 281-340, 1987.

[3] "Boston Dynamics," 2021. [Online]. Available: https://www.bostondynamics.com/spot.

[4] J. Kulk and J. Welsh, "A low power walk for the NAO robot," in *In Proceedings of the Australasian Conference on Robotics & Automation (ACRA),* 2008.

[5] J. Morales, J. L. Martinez, A. Mandow, A. J. Garcia-Cerezo and S. Pedraza, "Power consumption modeling of skid-steer tracked mobile robots on rigid terrain," *IEEE Transactions on Robotics,* vol. 25, no. 5, pp. 1098-1108, 2009.

[6] J. L. Martinez, A. Mandow, J. Morales, S. Pedraza and A. Garcia-Cerezo, "Approximating kinematics for tracked mobile robots," *The International Journal of Robotics Research,* vol. 24, no. 10, pp. 867-878, 2005.

[7] K. Tadakuma, R. Tadakuma, A. Maruyama, E. Rohmer, K. Nagatani, K. Yoshida, A. Ming, M. Shinojo, M. Higashimori and M. Kaneko, "Mechanical Design of the Wheel-Leg Hybrid Mobile Robot to Realize a Large Wheel Diameter," in *IEEE/RSJ International Conference on Intelligent Robots and Systems,* Taipei, Taiwan, 2010.

[8] D. Lee, G. Jung, M. Sin, S. Ahn and K. Cho, "Deformable Wheel Robot Based on Origami Structure," in *IEEE International Conference on Robotics and Automation*, Karlsruhe, Germany, 2013.

[9] T. Sun, X. Xiang, W. Su, H. Wu and Y. Song, "A transformable wheel-legged mobile robot: Design, analysis and," *Robotics and Autonomous Systems,* vol. 98, pp. 30-41, 2017.

[10] D. Y. Lee, S. R. Kim, J. S. Kim, J. J. P. Cho and K. J., "Origami Wheel Transformer: A Variable- Diameter Wheel Drive Robot Using an Origami Structure," *Soft Robotics,* vol. 00, no. 00, 2017.

[11] Y. She, C. Hurd and H. J. Su, "A Transformable Wheel Robot with a Passive Leg," in *IEEE/RSJ International Conference on Intelligent Robots and Systems (IROS)*, Hamburg, Germany, 2015.

[12] A. J. Clark, K. A. Cissell and J. M. Moore, "Evolving Controllers for a Transformable Wheel Mobile Robot," *Hindawi,* 2018.

[13] S. C. Chen, K. J. Huang, W. H. Chen, S. Y. Shen, C. H. Li and P. C. Lin, "Quattroped: A Leg- Wheel Transformable Robot," *IEEE/ASME TRANSACTIONS ON MECHATRONICS,*, vol. 19, no. 2, 2014.

[14] M. Ning, Z. Ma, H. Chen, J. Cao, C. Zhu, Y. Liu and Y. Wang, "Design and analysis for a multifunctional rescue robot with four- bar wheel- legged structure," *Advances in Mechanical Engineering,* vol. 10, no. 2, 2018.

[15] W. H. Chen, H. S. Lin, Y. M. Lin and P. C. Lin, "TurboQuad: A Novel Leg- Wheel TransformableRobot With Smooth and Fast Behavioral Transitions," *IEEE TRANSACTIONS ON ROBOTICS,* vol. 33, no. 5, 2017.

[16] Z. Wei, G. Song, G. Qiao, Y. Zhang and H. Sun, "Design and Implementation of a Leg-Wheel Robot: Transleg," *Journal of Mechanisms and Robotics*, vol. 9, 2017.

[17] F. Zhou, X. Xu, H. Xu, T. Z. Zhang and L. Zhang, "Transition mechanism design of a hybrid wheel- track- leg based on foldable rims," *Journal of Mechanical Engineering Science*, vol. 233, no. 13, pp. 4788-4801, 2019.

[18] S. S. Yun, J. Y. Lee, G. P. Jung and K. J. Cho, "Development of A Transformable Wheel Actuated by Soft Pneumatic Actuators," *International Journal of Control, Automation and Systems*, vol. 15, no. 1, pp. 36- 44, 2017.

[19] K. Tadakuma, R. Tadakuma, A. Maruyama, E. Rohmer, K. Nagatani, K. Yoshida, A. Ming, S. Makoto, M. Higashimori and M. Kaneko, "Armadillo-Inspired Wheel-Leg Retractable Module," in *International Conference on Robotics and Biomimetics*, Guilin, China, 2009.

[20] P. Liljeback, K. Y. Petterson, O. Stavdahl and J. T. Gravdahl, "Snake Robot Locomotion in Environments," *IEEE/ASME TRANSACTIONS ON MECHATRONICS*, vol. 17, no. 6, 2012.

[21] F. Michaud, D. Letourneau, M. Arsenault, Y. Bergeron, R. Cardin, F. Gagnon, M. A. Legault, M. Millete, J. F. Pare, M. C. Tremblay, P. Lepage, Y. Morin, J.Bisson and S. Caron, "Multi-Modal Locomotion Robotic Platform Using Leg- Track- Wheel Articulations," *Springer Science Autonomous Robots*, vol. 18, pp. 137-156, 2005.

[22] J. Smith, I. Sharf and M. Trentini, "PAW: a Hybrid Wheeled- Leg Robot," in *IEEE International Conference on Robotics and Automation*, Orlando, USA, 2006.

[23] I. Mertyuz, B. T. A. K. Tany1ld1z1, A. B. Tatar and O. Yakut, "FUHAR: A transformable wheel-legged hybrid mobile robot," *Robotics and Autonomous Systems,* vol. 133, 2020.

[24] J. J. Chou and L. S. Yang, "Innovative Design of a Claw- Wheel Transformable Robot," in *IEEE International Conference on Robotics and Automation (ICRA)*, Karlsruhe, Germany , 2013.

[25] Y. Kim, Y. Lee, S. Lee, J. Kim, H. S. Kim and T. Seo, "STEP: A New Mobile PlatformWIth 2- DOF Transformable Wheels for Service Robots," *IEEE/ASME Transactions on Mechatronics,* vol. 25, no. 4, 2020.

[26] Y. S. Kim, G. P. Jung, H. Kim, K. J. Cho and C. N. Chu, "Wheel Transformer: A Miniaturized Terrain Adaptive Robot with Passively Transformed Wheels," in *IEEE International Conference on Robotics and Automation (ICRA)*, Karlsruhe, Germany, 2013.

[27] L. Smith, R. D. Quinn, K. A. Johnson and W. R. Tuck, "The Tri- Wheel: A Novel Wheel-Leg Mobility Concept," in *IEEE/RSJ International Conference on Intelligent Robots and Systems (IROS)*, Hamburg, Germany, 2015.

[28] S. Ryu, Y. Lee and T. Seo, "Shape-Morphing Wheel Design and Analysis for Step Climbing in High Speed Locomotion," *IEEE ROBOTICS AND AUTOMATION LETTERS,* vol. 5, no. 2, 2020.

[29] L. Bai, J. Guan, X. Chen, J. Hou and W. Duan, "An optional passive/ active transformable wheel- legged mobilityconcept for serach and rescue robot," *Robotics and Autonomous Systems* , vol. 107, pp. 145-155, 2018.

[30] Y. Kim, J. Kim, H. S. Kim and T. Seo, "Curved- Spoke Tri- Wheel Mechanism for Fast Stair- Climbing," *IEEE Access,* vol. 7, 2019.

[31] X. Zhao, W. Su and S. Zhang, "The simulation and analysis of a new rescue robot with transformable wheels," in *2nd World Conference on Mechanical Engineering and Intelligent Manufacturing (WCMEIM)*, 2019.

[32] K. Kim, Y. Kim, J. Kim, H. S. Kim and T. Seo, "Optimal Trajectory Planning for 2- DOF Adaptive Transformable Wheel," *IEEE Access,* vol. 8, 2020.

[33] K. P. Sun, D. C. Yang, X. Chang, P. X. Lu, H. Zhu and K. Chen, "Design and Develepment of the Wheel- legged Robot Dog Kara," in *International Conference on Computer Science, Communications and Big Data (CSCBD 2019)*, 2019.

[34] C. Zheng and K. Lee, "WheeLeR: Wheel-Leg Reconfigurable Mechanism with Passive Gears for Mobile Robot Applications," in *International Conference on Robotics and Automation (ICRA)*, Montreal, Canada, 2019.

[35] Z. Bi, L. Wang, C. Wu, G. Yang and Z. D, "Multidisciplinary Design Optimization in Engineering," *Mathematical Problems in Engineering,* 2013.

[36] J. Agate, O. Weck, J. S.-. Sobieski, P. Aredensen, A. Morris and M. Spieck, "MDO: assesment and direction for advancement - an opinion of one inetrantional group," *Springer,* vol. 40, pp. 17-33, 2009.

[37] J. P. Giesing and J. F. M. Barthelemy, "A Summary of Industry MDO Applications and Needs," *American Institute of Aeronautics and Astronautics, Inc.*, 1998.

[38] D. J. Wilde and P. Papalambros, Principles of Optimal Design: Modeling and Computation, Cambridge University Press, 1998.

[39] V. B. Bhandari, Design of Machine Elements, McGraw Hill Education, 1994.

[40] R. N. Kacker, E. S. Lagergren and J. J. Filliben, "Taguchi's Orthogonal Arrays Are Classical Designs of Experiments," *J Res Natl Inst Stand Technol*, vol. 96, no. 5, 1991.

[41] "2018 International Building Code," ICC Digital Codes- International Code Council, 2018. [Online]. Available: https://codes.iccsafe.org/content/IbC2018.

[42] "Measuring Vibrations," ArduPilot, 2021. [Online]. Available: https://ardupilot.org/copter/docs/common-measuring-vibration.html.

[43] K. Lingaiah, Machine Design Data Book, McGraw Hill Education, 2003.